# Disruption of brainstem monoaminergic fibre tracts in multiple sclerosis as a putative mechanism for cognitive fatigue: a fixel-based analysis

Article (Accepted Version)

# Disruption of brainstem monoaminergic fibre tracts in multiple sclerosis as a putative mechanism for cognitive fatigue: a fixel-based analysis

Tiziana Carandini[1,2,*], Matteo Mancini[1,3,4], Iulia Bogdan[1], Charlotte L Rae[5], Andrew W Barritt[1], Arjun Sethi[6], Neil Harrison[7], Waqar Rashid[1], Elio Scarpini[2,8], Daniela Galimberti[2,8], Marco Bozzali[1,9], and Mara Cercignani[1,10].

[1]Department of Neuroscience, Brighton and Sussex Medical School, University of Sussex, UK.
[2]Fondazione IRCCS Ca' Granda Ospedale Maggiore Policlinico, Milan, Italy.
[3]NeuroPoly Lab, Polytechnique Montreal, Montreal, Canada.
[4]CUBRIC, Cardiff University, Cardiff, UK.
[5]School of Psychology, University of Sussex, UK.
[6]Psychiatry, Psychology & Neuroscience, King's College London, UK.
[7]Department of Psychology and Department of Medicine, Cardiff, UK.
[8]Department of Biomedical, Surgical and Dental Sciences, University of Milan, Dino Ferrari Center, Milan, Italy
[9]Rita Levi Montalcini Department of Neuroscience, University of Torino, Turin, Italy
[10]Neuroimaging Laboratory, Santa Lucia Foundation IRCCS, Rome, Italy.

***Corresponding Author**:
Tiziana Carandini
Fondazione IRCCS Ca' Granda Ospedale Maggiore Policlinico,
Milan, Italy
Email: tizianacarandini@gmail.com
Telephone: +39 02 5503 3845
ORCID: 0000-0002-0568-7580

**Keywords**
Multiple sclerosis, monoaminergic system, tractography, fixel-based analysis, fatigue

**Abstract**

In multiple sclerosis (MS), monoaminergic systems are altered as a result of both inflammation-dependent reduced synthesis and direct structural damage. Aberrant monoaminergic neurotransmission is increasingly considered a major contributor to fatigue pathophysiology. In this study, we aimed to compare the integrity of the monoaminergic white matter fibre tracts projecting from brainstem nuclei in a group of patients with MS (*n=68*) and healthy controls (*n=34*), and to investigate its association with fatigue. Fibre tracts integrity was assessed with the novel fixel-based analysis that simultaneously estimates axonal density, by means of 'fibre density', and white matter atrophy, by means of fibre 'cross section'. We focused on ventral tegmental area, locus coeruleus, and raphe nuclei as the main source of dopaminergic, noradrenergic, and serotoninergic fibres within the brainstem, respectively. Fourteen tracts of interest projecting from these brainstem nuclei were reconstructed using diffusion tractography, and compared by means of the product of fibre-density and cross-section (FDC). Finally, correlations of monoaminergic axonal damage with the modified fatigue impact scale scores were evaluated in MS. Fixel-based analysis revealed significant axonal damage – as measured by FDC reduction – within selective monoaminergic fibre-tracts projecting from brainstem nuclei in MS patients, in comparison to healthy controls; particularly within the dopaminergic-mesolimbic pathway, the noradrenergic-projections to prefrontal cortex, and serotoninergic-projections to cerebellum. Moreover, we observed significant correlations between severity of cognitive fatigue and axonal damage within the mesocorticolimbic tracts projecting from ventral tegmental area, as well as within the locus coeruleus projections to prefrontal cortex, suggesting a potential contribution of dopaminergic and noradrenergic pathways to central fatigue in MS. Our findings support the hypothesis that axonal damage along monoaminergic pathways contributes to the reduction/dysfunction of monoamines in MS and add new information on the mechanisms by which monoaminergic systems contribute to MS pathogenesis and fatigue. This supports the need for further research into monoamines as therapeutic targets aiming to combat and alleviate fatigue in MS.

## 1. Introduction

Multiple Sclerosis (MS) is a chronic demyelinating disease of the central nervous system (CNS). The complex pathogenesis of MS is still largely unknown with respect to dysregulation of the immune system that pathologically targets the CNS myelin and oligodendrocytes. In recent years, the investigation of MS pathogenesis has focused on the reciprocal interactions between the immune and the nervous systems (Melnikov et al., 2018). Monoamines are crucial for these interactions due to their capability of binding to cell receptors of both the innate and adaptive immune system (Melnikov et al., 2020). Monoamines encompass three main types of neurotransmitters: dopamine, noradrenaline, and serotonin. In the brain, monoamine-producing neurons are located within the brainstem monoaminergic nuclei (BrMn) and project diffusely to the whole CNS, crucially regulating normal brain function (Bär et al., 2016). Dopaminergic (DA)-cells are located in the substantia nigra and ventral tegmental area (VTA) that are the origins of the nigrostriatal and mesocorticolimbic systems, respectively. The mesolimbic pathway comprises projections from the VTA to the nucleus accumbens ($N_{acc}$) and the limbic system (particularly hippocampus and amygdala), while the mesocortical system links the midbrain with the prefrontal cortex (PFC) and the rest of the neocortex (Bär et al., 2016; Ikemoto, 2007). Noradrenergic (NA)-fibres originate from the locus coeruleus (LC) and distribute throughout all the brain, with PFC receiving the largest contingent (Liu et al., 2017). The median and dorsal raphe nuclei (MR and DR) are the main source of serotoninergic (5HT)-cells within the brainstem. Their efferent projections reach all cortical areas (Hornung, 2003) and richly innervate the cerebellum (Oostland and van Hooft, 2013). Monoaminergic systems are dysfunctional in many neurological and psychiatric diseases (Admon et al., 2017; Pavese et al., 2010; Serra et al., 2018), and represent the target for a large number of clinically efficacious drugs.

Monoamines are key mediators of neuroimmune interaction and influence MS pathogenesis and course (Levite et al., 2017; Malinova et al., 2018; Manjaly et al., 2019; Polak et al., 2011). Both peripheral and CNS inflammation reduces monoamines' synthesis and promotes a pro-inflammatory status in immune cells, increasing cytokine release and suppressing anti-inflammatory pathways (Cosentino et al., 2016; Melnikov et al., 2016). In addition to the direct effect of inflammation, brain monoamines in MS are reduced also as an indirect effect of structural damage. Brainstem is a major target of inflammation in MS and BrMn lesions are described with potential retrograde degeneration (Gadea, 2004; Polak et al., 2011; Tortorella et al., 2006). Moreover white matter (WM) damage leads to axonal loss within monoaminergic fibre tracts, possibly altering/reducing monoaminergic transmission in MS and

causing a dysregulation of monoaminergic pathways (Gadea, 2004; Levite et al., 2017; Madsen et al., 2017; Malinova et al., 2018; Manjaly et al., 2019; Polak et al., 2011; Simonini et al., 2010). The reduction/dysfunction of monoamines in MS may contribute to a wide range of clinical features typical of MS, such as fatigue, pain, and depression. Among them, fatigue is of particularly interest. Fatigue affects up to 80% of MS patients and represents one of the most debilitating symptoms (Heitmann et al., 2020; Manjaly et al., 2019). This is in part due to the fact that only few therapeutic options are available to alleviate the sensation of fatigue, ranging from pharmaceutical to non-pharmaceutical interventions (i.e. exercise, meditation and education) (Induruwa et al., 2012; Zielińska-Nowak et al., 2020). In general, there is a lack of consensus in treating MS fatigue, which might be attributable to deviations with regard to methods, MS populations and interventions. Moreover, one of the reasons for the difficulty in developing effective interventions is that, to date, the mechanisms underlying fatigue in MS are not completely understood (Manjaly et al., 2019; Zielińska-Nowak et al., 2020). Increasing evidence supports that altered monoaminergic neurotransmission and/or inflammation-induced decrease of neurotransmitter synthesis – with the consequent reduction of monoaminergic inputs supply to cortical/subcortical regions and the functional reorganisation of cortical networks – could contribute to MS fatigue (Dobryakova et al., 2015; Liu et al., 2017; Manjaly et al., 2019; Meeusen and Roelands, 2018; Pardini et al., 2010). In line with this monoaminergic hypothesis, two drugs currently used to treat fatigue in MS – amantadine and methylphenidate – are both DA-agonists (Zielińska-Nowak et al., 2020).

In this study, we aimed to investigate structural damage within monoaminergic WM fibre pathways in MS, as compared to healthy controls (HC). Brainstem monoaminergic fibre tracts integrity was assessed by means of diffusion-MRI and tractography. To analyse diffusion-MRI data, we used the novel fixel-based analysis (FBA) which provides quantitative measures of macro- and microstructure associated with a single fibre population, even in voxels containing crossing fibres (Mito et al., 2018; Raffelt et al., 2017). FBA utilizes constrained spherical deconvolution (CSD) to estimate the fibre orientation distribution (FOD) within each voxel (Tournier et al., 2007) and identify the underlying fibre populations, called “fixels” (Raffelt et al., 2017, 2015). This is particularly important when reconstructing fibers originating from the BrMn, which are small compared to the typical resolution of diffusion-MRI. FOD amplitude is proportional to the apparent fibre density (FD) of axons aligned in that direction within a WM bundle when derived from high b-value diffusion-MRI data (Gajamange et al., 2018; Raffelt et al., 2012). Through the non-linear FOD registration, FBA also provides information about the local morphology of WM tracts, called fibre cross-section (FC), which

reflects the volume perpendicular to the fibre orientation for each fibre population in a given voxel, not assessed with canonical approaches such as diffusion-tensor-imaging (Jeurissen et al., 2013). Finally, FD and FC values are multiplied to obtain the fibre density and cross-section (FDC) metric (FDC=FDxFC) that provides an overall picture of microstructural and macroscopic integrity across the WM tract. This has a fundamental importance in a disease like MS, where WM loss can result both from an alteration of intra-axonal volume of a fibre population within a voxel, and from axonal loss (atrophy) across the entire cross-section of the bundle (Gajamange et al., 2018; Ginsberg and Martin, 2002; Trapp and Stys, 2009). The contribution of macroscopic WM lesion load – particularly within the brainstem – and regional grey matter (GM) atrophy were also investigated by performing WM lesion probability maps and voxel-based morphometry, respectively. Finally, possible associations between monoaminergic fibre tracts axonal damage (as measured by FDC) and fatigue scores were investigated, in order to better understand the role of monoamines in the pathophysiology of MS fatigue.

## 2. Methods

### *2.1 Participants*

Sixty-eight patients with relapsing-remitting-MS (RR-MS) (Thompson et al., 2018) and 34 age- and sex-matched HC were recruited from the Brighton and Sussex Universities Hospitals Trust MS-clinic, UK. Patients were between 18 and 55 years-old and had an expanded disease status score (EDSS)<6.5 (Kurtzke, 1983). Exclusion criteria for patients were a history of other neurological diseases, psychiatric conditions and clinically significant disorders. Since mood and sleep disturbances may alter brainstem function, the Hospital Anxiety and Depression Scale (HADS-D) and the Epworth Sleepiness Scale (ESS) were used to exclude participants with evidence of depression and those likely to suffer from sleep disorders at the suggested cut-off of 11 and 10, respectively (Popp et al., 2017; Watson et al., 2014). MS patients were also screened for cognitive impairment, using the written version of the symbol digit modalities test of the brief International Cognitive Assessment for MS (Langdon et al., 2012). Further exclusion criteria included steroid treatment or MS relapses within the previous 4 weeks, as well as patients whose MS-treatment had been changed within that same interval. HC were between 18 and 70-year-old, without any significant medical disorders. Participants who had been on treatment with hypnotics within the last 4 weeks prior to their enrolment, on recreational drugs, or with a known alcohol abuse, were excluded.

Ethical approvals were obtained from the London-Surrey Borders Research Ethics Committee (REC reference 17/LO/0081) and the local BSMS-Research Governance and Ethics Committee (REC reference 14/014/HAR). Written informed consent was obtained from all participants before study initiation according to the declaration of Helsinki.

### *2.2 Fatigue assessment*

Fatigue was assessed using the Modified Fatigue Impact Scale (MFIS), a 21-item questionnaire that assesses impact on cognitive, physical, and psychosocial domains. The total MFIS score (MFIS-Tot; ranging 0-84) is computed by adding scores of the cognitive (MFIS-Cog), physical (MFIS-Phys), and psychosocial (MFIS-PS) subscales (Flachenecker et al., 2002). MFIS were administered to MS patients at visit 1 around 9-10 am, before neurological examination.

### *2.3 MRI acquisition*

MRI was performed in MS patients at visit 2 around noon. Visits 1 and 2 have been not more than two weeks apart. MRI data were acquired in all participants on a 1.5T Siemens Magnetom Avanto scanner (Siemens Healthcare Solutions, Erlangen, Germany) equipped with a 32-channel head-coil at the Clinical Imaging Sciences Centre of the University of Sussex, UK. The full examination included: 1) 2D-Dual-echo turbo-spin-echo (TSE; TEs=11/86ms, TR=3040ms, echo-train-length=6, flip-angle=150°, FoV=220x192mm$^2$; matrix=256x224; slice-thickness=5mm); 2) 2D-Fast fluid-attenuated inversion recovery (FLAIR; TE=87ms, TR=8000ms, TI=2500ms, flip-angle=150°, echo-train-length=17, same resolution as the dual echo); 3) 3D-Volumetric high-resolution T1-weighted magnetization prepared rapid gradient-echo (MPRAGE; TE=3.57ms; TR=27.30ms; TI=100ms; flip-angle=70°; FoV=256x240mm$^2$; matrix=254x40; slice-thickness=1mm); 4) 2D-2-shell diffusion-weighted pulsed-gradient spin-echo EPI (TE=95ms, TR=4036, b values=800/2000s/mm$^2$, number of diffusion directions=30/54, FoV=240x240mm$^2$, matrix=96x96, slice-thickness=2.5mm, additional 9 images with no diffusion weighting ($b_0$) were acquired). Part of the b0 volumes were acquired with reversed gradient blips to enable correcting for susceptibility artefacts (Andersson and Sotiropoulos, 2016). The duration of the diffusion-weighted MRI scan was approximately 14 minutes. In addition, resting-state functional-MRI data and quantitative magnetization transfer imaging data were collected but are not included in the analysis presented here. In total, the MRI session lasted 45 minutes.

*2.4 FBA: pre-processing of data and FOD calculation*

FBA was performed using the MRtrix3 package (Brain Research Institute, Melbourne, Australia; http://mrtrix.readthedocs.io/en/latest). We followed the suggested processing which can be found at: https://mrtrix.readthedocs.io/en/latest/fixel_based_analysis/mt_fibre_density_crosssection.html (Tournier et al., 2019). Pre-processing steps include data denoising and Gibbs ringing removal that were performed using MRtrix3 (Tournier et al., 2019). The diffusion-MRI data were then corrected for susceptibility and eddy-current distortions, as well as for involuntary movement using the tools *topup* and *eddy*, available with the FMRIB Software Library (FSL, https://fsl.fmrib.ox.ac.uk/fsl/fslwiki/eddy). Additionally, bias field correction was performed with MRtrix3 (Tournier et al., 2019). Data were upsampled to a voxel size of 1.25 mm isotropic to increase anatomical contrast and improve the downstream steps of template building, registration, tracking, and statistics. After the pre-processing, for each subject a whole-brain mask was defined and a FOD was computed from the highest b-value only (b=2000s/mm$^2$) using the Dhollander method (Dhollander T, Raffelt D, Connelly A, 2016). We chose to select only this b-value to avoid any potential extra-axonal signal contribution (Genc et al., 2020), as previously done in other studies (Dimond et al., 2020). The Dhollander method is designed to rely on multi-tissue CSD even in absence of multi-shell data (Dhollander T et al., 2019). Each subjects' mask was visually inspected to check whether all brain regions intended to be analysed were included. A population-averaged FOD template was generated combining the FODs from a representative subset of subjects in a midway space (20 MS-patients and 20 HC, randomly chosen), and then non-linearly registering the FOD of each subject (including the ones in the initial subset) to the template (Raffelt et al., 2012, 2011). Masks were warped to template space and the template was filtered using the intersection of all the subjects' masks in template space. Fixels were then segmented from the FOD template, generating the fixel template mask used in the subsequent statistical analyses (Raffelt et al., 2015).

*2.5 Fixel-based metrics*

FD, FC, and FDC were calculated for each subject across all WM fixels in the fixel template mask. FD was mapped for each subject directly from the template space as the integral of the FOD. A reduced FD may indicate fewer axons in a fixel, and therefore potential WM microstructural damage. The Jacobian determinant of the deformation field generated from the registration of each subject's FOD map to the FOD template was used to obtain the FC metric.

FC values higher than 1 indicate a larger FC in the participant as compared to the reference FOD template, while FC values lower than 1 indicate a smaller FC that may result from impaired axonal growth or atrophy after neuronal damage. In order to ensure that FC data were centred around zero and normally distributed, we used the natural logarithm of FC for group comparisons. FD and FC were finally multiplied by each fixel to obtain FDC values (FDC=FDxFC) (Raffelt et al., 2017).

*2.6 Tract of interest analysis*

A tract of interest analysis was conducted to investigate alterations in specific DA, NA, and 5HT fibre tracts (**Fig.1**). WM tracts between selected regions of interest (ROI) were probabilistically reconstructed using the iFOD2 algorithm implemented in MRtrix3, using the appropriate parameters to obtain results in line with the expected anatomy of each pathway. Tractography was performed from every voxel included in the seed regions. Tracts were then identified by imposing that each tract should either cross or reach other specified regions. These regions (as detailed in **Supplementary Table 1**) were chosen based on prior anatomical knowledge which have been supported by existing literature (Coenen et al., 2018; Counts and Mufson, 2012; Englot et al., 2018; Kline et al., 2016; Liu et al., 2017). Exclusion criteria by means of tailored ROI were used. ROI were created using the Harvard-Oxford cortical and structural atlases for cortical and subcortical structures, and the Probabilistic Atlas of the Human Cerebellum for cerebellar cortex, both distributed with FSL (Desikan et al., 2006; Diedrichsen et al., 2009). The atlases were aligned to the population template using a non-linear transformation estimated with the ANTs software package (http://stnava.github.io/ANTs/): first, we estimated a non-linear transformation using the 1 mm MNI template as the fixed image and the spherical harmonic of order l=0 from the FOD as the moving image (using the default parameters); then, we applied the inverse warp (from MNI to the FOD template) to align the ROIs to the population template. It is important to note that, although the volume of the BrMn is small, the tractography approach we have chosen, which allows multiple directions per voxels and uses a priori anatomical knowledge, limits the risk of including unwanted tracts in the analyses. Examples of tracts' reconstruction are provided in **Fig.2**.

In detail, we reconstructed the two major efferent DA-projections originating from VTA: the mesolimbic (through which DA projections target the $N_{acc}$, amygdala, and hippocampus) and the mesocortical pathway (through which DA projections target the PFC) (Bär et al., 2016; Kandel, E. R., Schwartz, J. H., & Jessell, T. M., 2000). VTA projections ascend the midbrain and converge in basal forebrain in the dorsal portion of the medial forebrain bundle (MFB),

through which DA-axons reach the limbic system and the PFC, over the anterior limb of the internal capsule (aIC). We reconstructed these WM tracts and further subdivided them into three different mesolimbic (VTA-$N_{acc}$, VTA-amygdala, and VTA-hippocampus) and three mesocortical bundles (VTA-dorsolateral(dl)PFC, VTA-medial orbitofrontal(mOf)PFC, and VTA-lateral orbitofrontal(lOf)PFC). For NA pathways, we reconstructed the major efferent bundle connecting the LC to the PFC, which ascends the midbrain ventrally, prosecutes in the dorsal portion of the MFB (with DA-neurons), and reaches the PFC over the aIC (Benarroch, 2009; Kandel, E. R., Schwartz, J. H., & Jessell, T. M., 2000). PFC projections were divided into three different bundles (LC-dlPFC, LC-mOfPFC, and LC-lOfPFC). Given the wide-spread 5HT innervation of the CNS, we decided to focus on the specific 5HT fibre-tracts projecting from the raphe nuclei to two different cerebellar cortex regions: the lobules V-VI – functionally connected with sensory-motor areas – and the lobule VII (encompassing the Crus I, Crus II, and the lobule VIIb), functionally connected with PFC and posterior-parietal cortex (O'Reilly et al., 2010). We reconstructed distinct tracts originating from DR and MR to reach the cerebellar lobules of interest (V-VI and VII) in two separate bundles, through the superior and middle cerebellar peduncle, respectively (Hornung, 2003; Oostland and van Hooft, 2013). A schematic of the fibre tracts that have been analysed is provided in **Fig.1**. Finally, for the purpose of validating the method of reconstruction, we chose to study the cingulum as a representative WM fibre tract that is anatomically well-characterized and not primary structurally connected with the brainstem monoaminergic projections. In summary, the following 14 tracts were reconstructed: VTA-$N_{acc}$; VTA-amygdala; VTA-hippocampus; VTA-dorsolateral(dl)PFC; VTA-medial orbitofrontal(mOf)PFC; VTA-lateral orbitofrontal(lOf)PFC; LC-dlPFC; LC-mOfPFC; LC-lOfPFC; MR-Cerebellar Lobule V-VI; MR-Cerebellar Lobule VII; DR-Cerebellar lobule V-VI; DR-Cerebellar lobule VII; cingulum. Averaged FD, FC, and FDC were calculated across the fixels in each tract in MS patients and HC.

*2.7 WM lesion identification and probability lesion map*

WM macroscopic lesions were identified on FLAIR scans by consensus between two observers and measured by using a local thresholding segmentation technique (Jim Image Analysis Package; Xinapse Systems, Leicester, UK). T2-weighted scans were used to increase confidence in lesion identification. Binary lesion maps were computed and warped into 1mm MNI space using ANTs. Lesion maps were then averaged across patients to yield a probability map where each voxel value represents the proportion of patients having a lesion in that given

voxel. For example, a value of 0.3 indicates that 30% of our cohort had a lesion in that specific location.

*2.8 Regional GM atrophy*

Every participant's MPRAGE was visually inspected to exclude macroscopic artefacts and segmented in Statistical Parametric Mapping 12 (SPM12; Wellcome Department of Imaging Neuroscience; www.fil.ion.ucl.ac.uk/spm) to obtain participant-specific GM, WM and CSF maps, as well as the total intracranial volume (TIV). Data were processed using an optimized VBM protocol (Ashburner and Friston, 2005; Good et al., 2001). Segmentation and normalization produced a GM probability map in Montreal Neurological Institute (MNI) coordinates. To compensate for compression or expansion during warping of images to match the template, GM maps were modulated by multiplying the intensity of each voxel by the local value derived from the deformation field. All data were then smoothed using a 8-mm full width half maximum Gaussian kernel. Regional differences in GM volume between HC and MS patients were assessed, with age, gender, and TIV as covariates of no interest. All analyses were conducted with SPM12 and tested at $p<0.05$ family-wise-error ($_{FWE}$), corrected at peak level.

*2.9 Statistical analyses*

SPSS-Statistics-v25.0 (SPSS Inc., Chicago, USA), and PRISM-v6.0 (GraphPad, San Diego, USA) were used for statistical analyses. Between-group comparisons of demographic variables were tested with Mann-Whitney U tests or chi-square tests, as appropriate, setting $p<0.05$. FBA results were represented as the mean FD/FC/FDC and standard deviation (SD) in MS-patients and HC. FC data are expressed as logarithm of FC values ($_{log}$FC) to ensure that data were centred around zero and normally distributed. Comparison between groups was tested with independent-sample t-tests, setting $p<0.003$ after Bonferroni correction for multiple comparisons (14 tracts: $\alpha=0.05/14=0.00357143$). Correlations between FDC and MFIS-Cog, MFIS-Phys and total MFIS scores were performed assessing the Pearson's correlation coefficient. We did not tested correlations between FDC and MFIS-PS due to lack of data in literature and difficulties in the interpretation of results concerning this subscale (Kos et al., 2005). As MFIS is computed as the sum of the subscores, and therefore is not independent, Bonferroni correction for multiple comparisons was applied considering 2 independent tests ((MFIS-Cog and MFIS-Phys), thus setting the threshold for significance at $p<0.025$ ($\alpha=0.05/2=0.025$).

## 3. Results

### *3.1 Participants' characteristics*

The main characteristics of the included population are summarized in **Table 1**. There were no significant differences between groups in age/gender distribution. Fifty-two of the recruited MS patients were on disease-modifying treatment (See **Table 1** for details), and 3 were under fatigue-treatment with amantadine for at least 5 years, with only 1 patient referring beneficial in alleviating fatigue.

### *3.2 FBA*

**Table 2** provides a detailed list of FBA results. Mesocorticolimbic DA-pathway was investigated. FBA revealed FDC reduction in the fibre tracts between VTA and $N_{acc}$, amygdala, and hippocampus in MS patients, compared to HC (**Fig. 3**). Notably, the VTA-$N_{acc}$ projection showed a reduction in both FD and FC. Conversely, FC was the only parameter reduced in the VTA-amygdala tract, and FD the only one reduced in the VTA-hippocampus tract. No significant difference in fixel metrics was observed in the tract between VTA and PFC between patients and HC, except for a slight reduction of FDC in the DA projections to lOfPFC and – to a minor extend – mOfPFC.

Projections from LC to PFC were investigated. A loss of FC and FDC within all fibre tracts connecting LC to PFC was found in MS patients, as compared to HC (**Fig. 4**). The LC-mOfPFC tract also showed lower FD values.

As concerns 5HT fibres, projections from the raphe nuclei to the cerebellar cortex were studied. FBA showed lower FDC in the tracts connecting both DR and MR to the cerebellar lobules V-VI and VII in MS patients, as compared to HC (**Fig. 5**), whereas no difference in average FD was found within the same tracts between the two groups. DR and MR projections to cerebellar lobules V-VI also showed reduced FC.

Although not reaching the statistical significance, FBA revealed that FC and FDC within the cingulum were reduced in MS patients, as compared to HC (**Supplementary Fig.1**).

### *3.3 WM-lesion incidence and regional GM atrophy*

The highest lesion incidence (>20%) was observed in the periventricular non-callosal-WM that includes the anterior, middle and posterior corona radiata, as well as in the thalamic radiation. Lesion frequency in the brainstem across all patients was less than 2% (i.e. only 1 out of 68 MS patients had visible brainstem WM lesions; **Fig. 6**). This suggests that the observed reductions in FBA-derived parameters are more likely to be explained by subtle axonal

degeneration and loss than by macroscopic lesions located within the BrMn. VBM analyses revealed no significant difference in global GM volume between MS patients and HC (mean±SD: 661.2±67.0 vs 686.4±69.9). When compared to HC, patients showed a significant regional GM loss in the thalamus bilaterally ($p_{FWE}$<0.0001; **Supplementary Fig.2)**.

*3.4 Associations between monoaminergic fibre-tract axonal loss and MS-fatigue*

BrMn axonal damage (by means of FDC reduction) was moderately associated with cognitive fatigue in MS. Particularly, MFIS-Cog inversely correlated with almost all the analysed DA tracts originating from VTA [$N_{acc}$ (r=-0.28; p=0.021), amygdala (r=-0.29; p=0.017), hippocampus (r=-0.36; p=0.002), mOfPFC (r=-0.25; p=not-significant), and lOfPFC (r=-0.30; p=0.014)]. Moreover, we found an inverse correlation between MFIS-cog and FDC within the LC-PFC tract [dlPFC (r=-0.29; p=0.017) and lOfPFC (r=-0.28; p=0.019)], but not within the WM tracts from DR/MR to cerebellar cortex, except a moderate correlation in the tract connecting MR to cerebellar-lobule VII (r=-0.27; p=0.025). No associations were found between FDC within all the analysed WM tracts and both MFIS-Tot and MFIS-Phys, except for a significant inverse correlation between FDC within the DA VTA-hippocampus tract and the MFIS-Tot score (r=-0.32, p=0.008). FDC within the cingulum resulted inversely correlated with MFIS-Cog (r=-0,34; p=0.004), as previously described (Bisecco et al., 2016). All correlation data are provided in **Supplementary Table 2**.

## 4. Discussion

The monoaminergic neurotransmitters dopamine, noradrenaline, and serotonin have a pivotal role in the interplay between the nervous and the immune system and are crucial regulators of normal brain function. Emerging evidence supports a dysregulation of monoaminergic systems in the pathogenesis of MS, secondary to both inflammation-induced reduction of monoamines' synthesis and structural damage to monoaminergic pathways within the brain. Only few studies have provided evidence of a structural damage of BrMn in MS (Polak et al., 2011), owning to the small dimension of the brainstem and its proximity to large arteries and ventricles. An indirect measure of monoaminergic structural damage in MS has been obtained with resting-state functional-MRI, by detecting functional disconnection between BrMn and other brain areas. Carotenuto et al. recently reported increased functional-connectivity between the dorsal raphe and the PFC, decreased functional-connectivity between the VTA and the PFC, and decreased betweenness centrality (a measure of the importance of a given node within a network) for the brainstem in MS patients, as compared to HC. These

findings suggest a damage in the ascending projections from BrMn in MS with a reduced activity in controlling the cortical regions of monoaminergic brain networks (Carotenuto et al., 2020). Similarly, by using proton-MRI-spectroscopy, Gadea et al. reported a reduction of N-acetyl-aspartate/creatine ratio in the pontine normal-appearing WM of a group of early RR-MS patients, possibly representing an indirect measure of structural damage of LC cells or its projections (Gadea, 2004).

Against this background, our study aimed to investigate whether these changes in functional connectivity are underpinned by a loss of structural connectivity. Specifically, we set out to evaluate the sensitivity of FBA-metrics (FD, FC, and FDC) as markers for axonal loss within specific DA, NA, and 5HT fibre-tracts in MS patients and HC. FBA has been recently applied in different pathologic conditions (Lyon et al., 2019; Mito et al., 2018; Pecheva et al., 2019; Raffelt et al., 2017). In MS, FBA was used by Gajamange et al. in a cohort of early MS patients with acute optic neuritis, finding reductions in fixel-based metrics in the visual pathway, as compared to HC (Gajamange et al., 2018). When comparing FBA to conventional diffusion-tensor imaging analysis, these Authors found a comparable sensitivity of FD and fractional anisotropy in detecting WM pathology in MS, but greater specificity for axonal density, higher sensitivity to damage in multiple fibre populations within a voxel, simultaneous measurement of microstructural and macroscopic neurodegenerative changes (Gajamange et al., 2018). This additional comprehensive analysis is precious in diseases like MS, where axonal damage within a given fibre-tract results from multiple factors, such as direct inflammatory injury with axonal transection and Wallerian retrograde degeneration; excitotoxicity-generated secondary axonal degeneration in denuded chronically-demyelinated axons; trans-synaptic degeneration resulting from the loss of afferent inputs or efferent targets (Gajamange et al., 2018; Ginsberg and Martin, 2002).

FBA revealed significant axonal damage within monoaminergic fibre-tracts projecting from BrMn in MS patients, in comparison to HC. The features of WM damage are different across individual tracts. As expected, considering that FD and FC are derived from two separate sources of information (diffusion signal and nonlinear transformation field respectively), the multiplication of their effects as FDC enabled an overall measure of fibre changes and provided the most significant data (Raffelt et al., 2017). Some fibre tracts (VTA projection to $N_{acc}$ and LC projections to mOfPFC) demonstrated both microstructural alterations in FD and macrostructural alterations in FC, revealing a pronounced structural disconnection between these BrMn and their cortical and subcortical efferent targets. VTA-hippocampus projections showed microstructural FD reduction, without substantial concomitant morphological

alterations within the fibre tract, suggesting that axonal loss occurs mainly at a microstructural level. Conversely, VTA projections to amygdala, LC projections to dlPFC and lOfPFC, raphe nuclei projections to cerebellar lobule V-VI, and PPN projections to cerebellar lobule V-VI displayed fibre tract-specific atrophy (as indexed by the FC metric), without changes in FD. Similarly, VTA-PFC projections showed a more substantial reduction in FC rather than both FD and FDC. This finding denotes a scenario where a difference in a fibre bundle's intra-axonal volume is manifested as a difference in the number of voxels that the fibre bundle occupies (Raffelt et al., 2017). It should be noted that from our analysis it seems that the macroscopic axonal loss (as expressed by FC) outweighs microscopic changes (as indicated in FD), and that FDC largely reflects FC. In summary, as concerns DA projections from VTA, MS patients showed significant axonal damage in the mesolimbic pathway, particularly in the fibre-tract targeting $N_{acc}$. The mesocortical tract displayed reduction in WM in MS patients in comparison of HC, although the difference did not reach statistical significance. This suggests a predominant involvement of the mesolimbic pathway in MS, as compared to the mesocortical pathway, that could be linked to topographical reasons, i.e. the preferential involvement of MS lesions for the deep periventricular WM/temporal horn of lateral ventricle (Arrambide et al., 2017). NA fibres projecting from LC to PFC showed in MS a significant WM reduction within all bundles taken into consideration, as compared to HC. Finally, MS patients displayed significant axonal damage within the 5HT fibre tracts from raphe nuclei targeting cerebellar lobules V-VI and from MR targeting cerebellar lobule VII. Taken all together, these results showed a disruption of brainstem monoaminergic fibre tracts integrity in MS, secondary to microscopic and/or macroscopic axonal loss. Only 1 out of 68 MS patients had visible macroscopic WM brainstem lesions, suggesting that local macroscopic lesions do not significantly contribute to our results. It should be noted, however, that the FLAIR acquisition had a slice thickness of 5mm, and therefore it is possible that we have missed some small brainstem lesions. Within this limitation, the prevalence of macroscopic WM lesions within the brainstem was too low to have an influence on fatigue. We have also assessed the pattern of GM loss, in order to establish its anatomical relationship with the WM pathways studied here. VBM showed a significant difference in GM volume between MS patients and HC only in bilateral thalamus, as already described (Bisecco et al., 2016; Filippi and Rocca, 2011). Therefore, regional GM atrophy is unlikely to contribute to axonal damage as assessed in this study.

Our study revealed also a moderate correlation between structural integrity within DA- and NA-WM tracts and the MFIS-cog, suggesting a link between structural damage within the

mesocorticolimbic and LC-PFC pathways and severity of central MS fatigue. Central fatigue is common in MS and is qualitatively different from peripheral fatigue, which primarily affects physical exercise, sparing mental processes (Arm et al., 2019). Our results are consistent with previous literature sustaining a role of aberrant monoaminergic – particularly DA – neurotransmission in the pathophysiology of MS fatigue (Dobryakova et al., 2015; Manjaly et al., 2019). Structural WM damage within monoaminergic pathways or inflammation-induced decrease of monoamines synthesis could explain the reduction in motivation, mood and arousal that characterize fatigue. Moreover, two drugs that are currently used to treat fatigue in MS – amantadine and methylphenidate – are both DA-agonists. Only 3 of the patients include in this study were under treatment with amantadine for fatigue (for a long-time). Although this could be seen as a confound in our analysis, the small number of patients who had been taking amantadine suggests that such an effect should be negligible. The dopamine imbalance hypothesis of fatigue in MS is supported by several imaging studies showing the presence of both structural and functional alterations within the mesocorticolimbic pathways of MS patients experiencing fatigue (Dobryakova et al., 2015; Genova et al., 2013; Pardini et al., 2010). Recently, Chen et al. demonstrated by using functional-MRI altered cognitive fatigue-related functional connectivity in the monoamine-associated interoceptive and reward pathways in MS and speculated that such alterations may be the result of inefficient brain connectivity when meeting increased task demands (Chen et al., 2020). Similarly, Jaeger et al performed a sub-region functional-MRI analysis finding that MS-related fatigue was associated with impaired functional connectivity of the striatum with sensorimotor, attention, and reward networks. Authors suggested the superior ventral striatum as the key integrational hub impaired in MS-related fatigue (Jaeger et al., 2019). Our data suggests a potential role of both dopamine and noradrenaline in the pathogenesis of MS fatigue that needs to be further investigated in future studies. Finally, although alterations of the 5HT system have been associated to fatigue (Dobryakova et al., 2015; Hesse et al., 2014), we did not report significant correlation (except for a trend toward significance in the tract connecting MR to cerebellar-lobule VII), possibly due to the fact that we only investigated those bundles originating from raphe nuclei and projecting to the cerebellar cortex.

Some limitations should be disclosed. First, the definition of BrMn using a standard space (MNI) atlas (due to the difficulties in identifying each nucleus on subject specific MRI) is less accurate than registering the standard ROI to each participant's scan and that BrMn' macroscopic atrophy might have affected our results (Serra et al., 2018). Nevertheless, it is not possible to measure each nucleus-volume independently to adjust for this potential confound.

A related point are the well-known limitations of tractography (Jones et al., 2013; Jones and Cercignani, 2010), especially in terms of potential false positives in the reconstructed tracts (Maier-Hein et al., 2017). To reduce this issue, a recent work has showed using an animal model how tractography can be highly accurate if one relies on prior anatomical knowledge (Schilling et al., 2020): in this direction, we leveraged anatomy to define constraints on a pathway-by-pathways basis and ultimately to reconstruct known connections of the brainstem nuclei. With respect to the interpretation of results, although we did not identify a significant amount of macroscopic lesions within the brainstem, we can not exclude that microstructural WM damage within the brainstem might have contributed to fatigue in our cohort of MS patients. The lack of fatigue and other clinical assessments in the control group could also be seen as a limitation and might have influenced our findings. However, HC were included only if they did not have any significant medical issue, and no neurological, psychiatric, and sleep disturbances. Fatigue is a pathological symptom that can be present in different diseases, especially inflammatory disorders, but it is not supposed to be present in the healthy population. Moreover, we are aware that mood and sleep disturbances may contribute to fatigue and be influenced by monoaminergic dysfunction in MS. For these reasons, we decide to exclude from the study all participants with evidence of depression and those likely to suffer from sleep disorders, by using specific validated scales (HADS-D and ESS). Moreover, the partial correlations between FDC and fatigue scores, controlling for depression and sleep disturbances (i.e. the individual scores of HADS-D and ESS) showed the same significant data (**Supplementary Table 3**). Similarly, all correlations between age and all MFIS scores did not show any significant association (all $p>0.05$). Although the study was designed to perform all the assessments at the same time of day for all participants, in some cases it was not possible to stick to rigid timing because it very much depended on people's availability. However, we should stress that this happened in a minority of cases, and anyhow we were mainly interested in trait fatigue, rather than state fatigue, which should not be affected too badly by time of assessment. Finally, the present study has a cross-sectional design. Longitudinal studies are needed to analyse the contribution of monoamines to MS pathogenesis and the relationship between monoaminergic pathways and fatigue modifications in MS.

### *4.1 Conclusions*

In conclusion, we have first used FBA to detect reduction of FDC within specific monoaminergic fibre tracts projecting from BrMn in MS, particularly within the DA-mesolimbic pathway, NA-projections to PFC and 5HT-projections to cerebellum. These

findings support the hypothesis that axonal damage along monoaminergic pathways contributes to the reduction/dysfunction of monoamines in MS and add new information on the mechanisms by which monoaminergic systems contribute to MS pathogenesis. Moreover, our study supports the hypothesis of a major contribution of the DA-mesocorticolimbic pathway to central fatigue in MS, and suggests a potential implication of the NA-LC-PFC pathway, possibly due to axonal loss that imbalances DA and NA neurotransmission. Although the relationship between aberrant monoaminergic neurotransmission and axonal loss in MS needs to be further clarified, our data support the need for further research into monoamines as potential therapeutic targets aimed to combat and alleviate fatigue in MS.

**CRediT authorship contribution statement**

**Tiziana Carandini**: Conceptualization, Formal analysis, Writing - original draft. **Matteo Mancini**: Conceptualization, Formal analysis, Writing - original draft. **Iulia Bogdan**: Project administration, Funding acquisition, Formal analysis. **Charlotte L Rae**: Funding acquisition, Formal analysis. **Andrew W Barritt**: Project administration, Formal analysis. **Arjun Sethi**: Formal analysis. **Neil Harrison**: Writing - review & editing. **Waqar Rashid**: Project administration, Formal analysis. **Elio Scarpini**: Writing - review & editing. **Daniela Galimberti**: Writing - review & editing. **Marco Bozzali**: Conceptualization, Writing - review & editing. **Mara Cercignani**: Conceptualization, Formal analysis, Project administration, Funding acquisition, Writing - original draft.

**Conflicts of interest:** the author(s) declared the following potential conflicts of interest with respect to the research, authorship, and/or publication of this article: MM was funded by the Wellcome Trust through a Sir Henry Wellcome Postdoctoral Fellowship (213722/Z/18/Z). IB received travel and study support from Biogen, Merck, Novartis and Sanofi-Genzyme. NH has served on scientific advisory boards for Janssen and GSK Pharmaceuticals, is in receipt of grant funding from the Wellcome Trust and has received research funding support from Janssen Pharmaceutics and Action for ME. MB received honoraria from Biogen and Merk, and research support from the Italian Ministry of Health. MC received royalties from Taylor and Francis from the publication of a book, research funding from Wellcome Trust, Motor Neuron Disease Association, and the Academy of Medical Sciences. She also received institutional support from the University of Sussex and the University of Brighton. TC, CLR, AWM, AS, WR, ES, and DG report no potential conflicts of interest.

**Funding:** the authors have not declared a specific grant for this research from any funding agency in the public, commercial or not-for-profit sectors.

**Appendix A. Supplementary data**

Supplementary data to this article can be found online

**References**

Admon, R., Kaiser, R.H., Dillon, D.G., Beltzer, M., Goer, F., Olson, D.P., Vitaliano, G., Pizzagalli, D.A., 2017. Dopaminergic Enhancement of Striatal Response to Reward in Major Depression. AJP 174, 378–386. https://doi.org/10.1176/appi.ajp.2016.16010111

Andersson, J.L.R., Sotiropoulos, S.N., 2016. An integrated approach to correction for off-resonance effects and subject movement in diffusion MR imaging. NeuroImage 125, 1063–1078. https://doi.org/10.1016/j.neuroimage.2015.10.019

Arm, J., Ribbons, K., Lechner-Scott, J., Ramadan, S., 2019. Evaluation of MS related central fatigue using MR neuroimaging methods: Scoping review. Journal of the Neurological Sciences 400, 52–71. https://doi.org/10.1016/j.jns.2019.03.007

Arrambide, G., Tintore, M., Auger, C., Río, J., Castilló, J., Vidal-Jordana, A., Galán, I., Nos, C., Comabella, M., Mitjana, R., Mulero, P., de Barros, A., Rodríguez-Acevedo, B., Midaglia, L., Sastre-Garriga, J., Rovira, A., Montalban, X., 2017. Lesion topographies in multiple sclerosis diagnosis: A reappraisal. Neurology 89, 2351–2356. https://doi.org/10.1212/WNL.0000000000004715

Ashburner, J., Friston, K.J., 2005. Unified segmentation. NeuroImage 26, 839–851. https://doi.org/10.1016/j.neuroimage.2005.02.018

Bär, K.-J., de la Cruz, F., Schumann, A., Koehler, S., Sauer, H., Critchley, H., Wagner, G., 2016. Functional connectivity and network analysis of midbrain and brainstem nuclei. NeuroImage 134, 53–63. https://doi.org/10.1016/j.neuroimage.2016.03.071

Benarroch, E.E., 2009. The locus ceruleus norepinephrine system: Functional organization and potential clinical significance. Neurology 73, 1699–1704. https://doi.org/10.1212/WNL.0b013e3181c2937c

Bisecco, A., Caiazzo, G., d'Ambrosio, A., Sacco, R., Bonavita, S., Docimo, R., Cirillo, M., Pagani, E., Filippi, M., Esposito, F., Tedeschi, G., Gallo, A., 2016. Fatigue in multiple sclerosis: The contribution of occult white matter damage. Mult Scler 22, 1676–1684. https://doi.org/10.1177/1352458516628331

Carotenuto, A., Wilson, H., Giordano, B., Caminiti, S.P., Chappell, Z., Williams, S.C.R.,

Hammers, A., Silber, E., Brex, P., Politis, M., 2020. Impaired connectivity within neuromodulatory networks in multiple sclerosis and clinical implications. J Neurol. https://doi.org/10.1007/s00415-020-09806-3

Chen, M.H., DeLuca, J., Genova, H.M., Yao, B., Wylie, G.R., 2020. Cognitive Fatigue Is Associated with Altered Functional Connectivity in Interoceptive and Reward Pathways in Multiple Sclerosis. Diagnostics (Basel) 10. https://doi.org/10.3390/diagnostics10110930

Coenen, V.A., Schumacher, L.V., Kaller, C., Schlaepfer, T.E., Reinacher, P.C., Egger, K., Urbach, H., Reisert, M., 2018. The anatomy of the human medial forebrain bundle: Ventral tegmental area connections to reward-associated subcortical and frontal lobe regions. NeuroImage: Clinical 18, 770–783. https://doi.org/10.1016/j.nicl.2018.03.019

Cosentino, M., Zaffaroni, M., Legnaro, M., Bombelli, R., Schembri, L., Baroncini, D., Bianchi, A., Clerici, R., Guidotti, M., Banfi, P., Bono, G., Marino, F., 2016. Dopaminergic receptors and adrenoceptors in circulating lymphocytes as putative biomarkers for the early onset and progression of multiple sclerosis. Journal of Neuroimmunology 298, 82–89. https://doi.org/10.1016/j.jneuroim.2016.07.008

Counts, S.E., Mufson, E.J., 2012. Locus Coeruleus, in: The Human Nervous System. Elsevier, pp. 425–438. https://doi.org/10.1016/B978-0-12-374236-0.10012-4

Desikan, R.S., Ségonne, F., Fischl, B., Quinn, B.T., Dickerson, B.C., Blacker, D., Buckner, R.L., Dale, A.M., Maguire, R.P., Hyman, B.T., Albert, M.S., Killiany, R.J., 2006. An automated labeling system for subdividing the human cerebral cortex on MRI scans into gyral based regions of interest. NeuroImage 31, 968–980. https://doi.org/10.1016/j.neuroimage.2006.01.021

Dhollander T, Mito R, Raffelt D, Connelly A, 2019. Improved white matter response function estimation for 3-tissue constrained spherical deconvolution. Abstract at the 27th International Society of Magnetic Resonance in Medicine, 2019, 27, 555.

Dhollander T, Raffelt D, Connelly A, 2016. Unsupervised 3-tissue response function estimation from single-shell or multi-shell diffusion MR data without a co-registered T1 image. Abstract at the ISMRM Workshop on Breaking the Barriers of Diffusion MRI, 2016, 5.

Diedrichsen, J., Balsters, J.H., Flavell, J., Cussans, E., Ramnani, N., 2009. A probabilistic MR atlas of the human cerebellum. NeuroImage 46, 39–46. https://doi.org/10.1016/j.neuroimage.2009.01.045

Dimond, D., Rohr, C.S., Smith, R.E., Dhollander, T., Cho, I., Lebel, C., Dewey, D., Connelly, A., Bray, S., 2020. Early childhood development of white matter fiber density and morphology. NeuroImage 210, 116552. https://doi.org/10.1016/j.neuroimage.2020.116552

Dobryakova, E., Genova, H.M., DeLuca, J., Wylie, G.R., 2015. The Dopamine Imbalance Hypothesis of Fatigue in Multiple Sclerosis and Other Neurological Disorders. Front. Neurol. 6. https://doi.org/10.3389/fneur.2015.00052

Englot, D.J., Gonzalez, H.F.J., Reynolds, B.B., Konrad, P.E., Jacobs, M.L., Gore, J.C., Landman, B.A., Morgan, V.L., 2018. Relating structural and functional brainstem connectivity to disease measures in epilepsy. Neurology 91, e67–e77. https://doi.org/10.1212/WNL.0000000000005733

Filippi, M., Rocca, M.A., 2011. The role of magnetic resonance imaging in the study of multiple sclerosis: diagnosis, prognosis and understanding disease pathophysiology. Acta Neurol Belg 111, 89–98.

Flachenecker, P., Kümpfel, T., Kallmann, B., Gottschalk, M., Grauer, O., Rieckmann, P., Trenkwalder, C., Toyka, K.V., 2002. Fatigue in multiple sclerosis: a comparison of different rating scales and correlation to clinical parameters. Mult Scler 8, 523–526. https://doi.org/10.1191/1352458502ms839oa

Gadea, M., 2004. Spectroscopic axonal damage of the right locus coeruleus relates to selective attention impairment in early stage relapsing-remitting multiple sclerosis. Brain 127, 89–98. https://doi.org/10.1093/brain/awh002

Gajamange, S., Raffelt, D., Dhollander, T., Lui, E., van der Walt, A., Kilpatrick, T., Fielding, J., Connelly, A., Kolbe, S., 2018. Fibre-specific white matter changes in multiple sclerosis patients with optic neuritis. NeuroImage: Clinical 17, 60–68. https://doi.org/10.1016/j.nicl.2017.09.027

Genc, S., Tax, C.M.W., Raven, E.P., Chamberland, M., Parker, G.D., Jones, D.K., 2020. Impact of *b* -value on estimates of apparent fibre density. Hum Brain Mapp 41, 2583–2595. https://doi.org/10.1002/hbm.24964

Genova, H.M., Rajagopalan, V., DeLuca, J., Das, A., Binder, A., Arjunan, A., Chiaravalloti, N., Wylie, G., 2013. Examination of Cognitive Fatigue in Multiple Sclerosis using Functional Magnetic Resonance Imaging and Diffusion Tensor Imaging. PLoS ONE 8, e78811. https://doi.org/10.1371/journal.pone.0078811

Ginsberg, S.D., Martin, L.J., 2002. Axonal transection in adult rat brain induces transsynaptic apoptosis and persistent atrophy of target neurons. J. Neurotrauma 19, 99–109. https://doi.org/10.1089/089771502753460277

Good, C.D., Johnsrude, I.S., Ashburner, J., Henson, R.N.A., Friston, K.J., Frackowiak, R.S.J., 2001. A Voxel-Based Morphometric Study of Ageing in 465 Normal Adult Human Brains. NeuroImage 14, 21–36. https://doi.org/10.1006/nimg.2001.0786

Heitmann, H., Andlauer, T.F.M., Korn, T., Mühlau, M., Henningsen, P., Hemmer, B., Ploner, M., 2020. Fatigue, depression, and pain in multiple sclerosis: How neuroinflammation translates into dysfunctional reward processing and anhedonic symptoms. Mult Scler 1352458520972279. https://doi.org/10.1177/1352458520972279

Hesse, S., Moeller, F., Petroff, D., Lobsien, D., Luthardt, J., Regenthal, R., Becker, G.-A., Patt, M., Thomae, E., Seese, A., Meyer, P.M., Bergh, F.T., Sabri, O., 2014. Altered serotonin transporter availability in patients with multiple sclerosis. Eur J Nucl Med Mol Imaging 41, 827–835. https://doi.org/10.1007/s00259-013-2636-z

Hornung, J.-P., 2003. The human raphe nuclei and the serotonergic system. J. Chem. Neuroanat. 26, 331–343.

Ikemoto, S., 2007. Dopamine reward circuitry: two projection systems from the ventral midbrain to the nucleus accumbens-olfactory tubercle complex. Brain Res Rev 56, 27–78. https://doi.org/10.1016/j.brainresrev.2007.05.004

Induruwa, I., Constantinescu, C.S., Gran, B., 2012. Fatigue in multiple sclerosis — A brief review. Journal of the Neurological Sciences 323, 9–15. https://doi.org/10.1016/j.jns.2012.08.007

Jaeger, S., Paul, F., Scheel, M., Brandt, A., Heine, J., Pach, D., Witt, C.M., Bellmann-Strobl, J., Finke, C., 2019. Multiple sclerosis-related fatigue: Altered resting-state functional connectivity of the ventral striatum and dorsolateral prefrontal cortex. Mult Scler 25, 554–564. https://doi.org/10.1177/1352458518758911

Jeurissen, B., Leemans, A., Tournier, J.-D., Jones, D.K., Sijbers, J., 2013. Investigating the prevalence of complex fiber configurations in white matter tissue with diffusion magnetic resonance imaging: Prevalence of Multifiber Voxels in WM. Hum. Brain Mapp 34, 2747–2766. https://doi.org/10.1002/hbm.22099

Jones, D.K., Cercignani, M., 2010. Twenty-five pitfalls in the analysis of diffusion MRI data. NMR Biomed. 23, 803–820. https://doi.org/10.1002/nbm.1543

Jones, D.K., Knösche, T.R., Turner, R., 2013. White matter integrity, fiber count, and other fallacies: The do's and don'ts of diffusion MRI. NeuroImage 73, 239–254. https://doi.org/10.1016/j.neuroimage.2012.06.081

Kandel, E. R., Schwartz, J. H., & Jessell, T. M., 2000. Principles of neural science., 6th edition. ed. New York: McGraw-Hill, Health Professions Division.

Kline, R.L., Zhang, S., Farr, O.M., Hu, S., Zaborszky, L., Samanez-Larkin, G.R., Li, C.-S.R., 2016. The Effects of Methylphenidate on Resting-State Functional Connectivity of the Basal Nucleus of Meynert, Locus Coeruleus, and Ventral Tegmental Area in Healthy Adults.

Front. Hum. Neurosci. 10. https://doi.org/10.3389/fnhum.2016.00149

Kos, D., Kerckhofs, E., Carrea, I., Verza, R., Ramos, M., Jansa, J., 2005. Evaluation of the Modified Fatigue Impact Scale in four different European countries. Mult Scler 11, 76–80. https://doi.org/10.1191/1352458505ms1117oa

Kurtzke, J.F., 1983. Rating neurologic impairment in multiple sclerosis: an expanded disability status scale (EDSS). Neurology 33, 1444–1452. https://doi.org/10.1212/wnl.33.11.1444

Langdon, D., Amato, M., Boringa, J., Brochet, B., Foley, F., Fredrikson, S., Hämäläinen, P., Hartung, H.-P., Krupp, L., Penner, I., Reder, A., Benedict, R., 2012. Recommendations for a Brief International Cognitive Assessment for Multiple Sclerosis (BICAMS). Mult Scler 18, 891–898. https://doi.org/10.1177/1352458511431076

Levite, M., Marino, F., Cosentino, M., 2017. Dopamine, T cells and multiple sclerosis (MS). J Neural Transm 124, 525–542. https://doi.org/10.1007/s00702-016-1640-4

Liu, K.Y., Marijatta, F., Hämmerer, D., Acosta-Cabronero, J., Düzel, E., Howard, R.J., 2017. Magnetic resonance imaging of the human locus coeruleus: A systematic review. Neuroscience & Biobehavioral Reviews 83, 325–355. https://doi.org/10.1016/j.neubiorev.2017.10.023

Lyon, M., Welton, T., Varda, A., Maller, J.J., Broadhouse, K., Korgaonkar, M.S., Koslow, S.H., Williams, L.M., Gordon, E., Rush, A.J., Grieve, S.M., 2019. Gender-specific structural abnormalities in major depressive disorder revealed by fixel-based analysis. NeuroImage: Clinical 21, 101668. https://doi.org/10.1016/j.nicl.2019.101668

Madsen, P.M., Sloley, S.S., Vitores, A.A., Carballosa-Gautam, M.M., Brambilla, R., Hentall, I.D., 2017. Prolonged stimulation of a brainstem raphe region attenuates experimental autoimmune encephalomyelitis. Neuroscience 346, 395–402. https://doi.org/10.1016/j.neuroscience.2017.01.037

Maier-Hein, K.H., Neher, P.F., Houde, J.-C., Côté, M.-A., Garyfallidis, E., Zhong, J., Chamberland, M., Yeh, F.-C., Lin, Y.-C., Ji, Q., Reddick, W.E., Glass, J.O., Chen, D.Q., Feng, Y., Gao, C., Wu, Y., Ma, J., He, R., Li, Q., Westin, C.-F., Deslauriers-Gauthier, S., González, J.O.O., Paquette, M., St-Jean, S., Girard, G., Rheault, F., Sidhu, J., Tax, C.M.W., Guo, F., Mesri, H.Y., Dávid, S., Froeling, M., Heemskerk, A.M., Leemans, A., Boré, A., Pinsard, B., Bedetti, C., Desrosiers, M., Brambati, S., Doyon, J., Sarica, A., Vasta, R., Cerasa, A., Quattrone, A., Yeatman, J., Khan, A.R., Hodges, W., Alexander, S., Romascano, D., Barakovic, M., Auría, A., Esteban, O., Lemkaddem, A., Thiran, J.-P., Cetingul, H.E., Odry, B.L., Mailhe, B., Nadar, M.S., Pizzagalli, F., Prasad, G., Villalon-Reina, J.E., Galvis, J., Thompson, P.M., Requejo, F.D.S., Laguna, P.L., Lacerda, L.M., Barrett, R., Dell'Acqua,

F., Catani, M., Petit, L., Caruyer, E., Daducci, A., Dyrby, T.B., Holland-Letz, T., Hilgetag, C.C., Stieltjes, B., Descoteaux, M., 2017. The challenge of mapping the human connectome based on diffusion tractography. Nat Commun 8, 1349. https://doi.org/10.1038/s41467-017-01285-x

Malinova, T.S., Dijkstra, C.D., de Vries, H.E., 2018. Serotonin: A mediator of the gut–brain axis in multiple sclerosis. Mult Scler 24, 1144–1150. https://doi.org/10.1177/1352458517739975

Manjaly, Z.-M., Harrison, N.A., Critchley, H.D., Do, C.T., Stefanics, G., Wenderoth, N., Lutterotti, A., Müller, A., Stephan, K.E., 2019. Pathophysiological and cognitive mechanisms of fatigue in multiple sclerosis. J Neurol Neurosurg Psychiatry 90, 642–651. https://doi.org/10.1136/jnnp-2018-320050

Meeusen, R., Roelands, B., 2018. Fatigue: Is it all neurochemistry? European Journal of Sport Science 18, 37–46. https://doi.org/10.1080/17461391.2017.1296890

Melnikov, M., Belousova, O., Murugin, V., Pashenkov, M., Boyко, A., 2016. The role of dopamine in modulation of Th-17 immune response in multiple sclerosis. Journal of Neuroimmunology 292, 97–101. https://doi.org/10.1016/j.jneuroim.2016.01.020

Melnikov, M., Rogovskii, V., Boyko, A., Pashenkov, M., 2018. The influence of biogenic amines on Th17-mediated immune response in multiple sclerosis. Multiple Sclerosis and Related Disorders 21, 19–23. https://doi.org/10.1016/j.msard.2018.02.012

Melnikov, M., Rogovskii, V., Boyko, A., Pashenkov, M., 2020. Dopaminergic Therapeutics in Multiple Sclerosis: Focus on Th17-Cell Functions. J Neuroimmune Pharmacol 15, 37–47. https://doi.org/10.1007/s11481-019-09852-3

Mito, R., Raffelt, D., Dhollander, T., Vaughan, D.N., Tournier, J.-D., Salvado, O., Brodtmann, A., Rowe, C.C., Villemagne, V.L., Connelly, A., 2018. Fibre-specific white matter reductions in Alzheimer's disease and mild cognitive impairment. Brain 141, 888–902. https://doi.org/10.1093/brain/awx355

Oostland, M., van Hooft, J.A., 2013. The role of serotonin in cerebellar development. Neuroscience 248, 201–212. https://doi.org/10.1016/j.neuroscience.2013.05.029

O'Reilly, J.X., Beckmann, C.F., Tomassini, V., Ramnani, N., Johansen-Berg, H., 2010. Distinct and Overlapping Functional Zones in the Cerebellum Defined by Resting State Functional Connectivity. Cerebral Cortex 20, 953–965. https://doi.org/10.1093/cercor/bhp157

Pardini, M., Bonzano, L., Mancardi, G.L., Roccatagliata, L., 2010. Frontal networks play a role in fatigue perception in multiple sclerosis. Behavioral Neuroscience 124, 329–336. https://doi.org/10.1037/a0019585

Pavese, N., Metta, V., Bose, S.K., Chaudhuri, K.R., Brooks, D.J., 2010. Fatigue in Parkinson's disease is linked to striatal and limbic serotonergic dysfunction. Brain 133, 3434–3443. https://doi.org/10.1093/brain/awq268

Pecheva, D., Tournier, J.-D., Pietsch, M., Christiaens, D., Batalle, D., Alexander, D.C., Hajnal, J.V., Edwards, A.D., Zhang, H., Counsell, S.J., 2019. Fixel-based analysis of the preterm brain: Disentangling bundle-specific white matter microstructural and macrostructural changes in relation to clinical risk factors. NeuroImage: Clinical 23, 101820. https://doi.org/10.1016/j.nicl.2019.101820

Polak, P.E., Kalinin, S., Feinstein, D.L., 2011. Locus coeruleus damage and noradrenaline reductions in multiple sclerosis and experimental autoimmune encephalomyelitis. Brain 134, 665–677. https://doi.org/10.1093/brain/awq362

Popp, R.F.J., Fierlbeck, A.K., Knüttel, H., König, N., Rupprecht, R., Weissert, R., Wetter, T.C., 2017. Daytime sleepiness versus fatigue in patients with multiple sclerosis: A systematic review on the Epworth sleepiness scale as an assessment tool. Sleep Medicine Reviews 32, 95–108. https://doi.org/10.1016/j.smrv.2016.03.004

Raffelt, D., Tournier, J.-D., Fripp, J., Crozier, S., Connelly, A., Salvado, O., 2011. Symmetric diffeomorphic registration of fibre orientation distributions. NeuroImage 56, 1171–1180. https://doi.org/10.1016/j.neuroimage.2011.02.014

Raffelt, D., Tournier, J.-D., Rose, S., Ridgway, G.R., Henderson, R., Crozier, S., Salvado, O., Connelly, A., 2012. Apparent Fibre Density: A novel measure for the analysis of diffusion-weighted magnetic resonance images. NeuroImage 59, 3976–3994. https://doi.org/10.1016/j.neuroimage.2011.10.045

Raffelt, D.A., Smith, R.E., Ridgway, G.R., Tournier, J.-D., Vaughan, D.N., Rose, S., Henderson, R., Connelly, A., 2015. Connectivity-based fixel enhancement: Whole-brain statistical analysis of diffusion MRI measures in the presence of crossing fibres. NeuroImage 117, 40–55. https://doi.org/10.1016/j.neuroimage.2015.05.039

Raffelt, D.A., Tournier, J.-D., Smith, R.E., Vaughan, D.N., Jackson, G., Ridgway, G.R., Connelly, A., 2017. Investigating white matter fibre density and morphology using fixel-based analysis. NeuroImage 144, 58–73. https://doi.org/10.1016/j.neuroimage.2016.09.029

Schilling, K.G., Petit, L., Rheault, F., Remedios, S., Pierpaoli, C., Anderson, A.W., Landman, B.A., Descoteaux, M., 2020. Brain connections derived from diffusion MRI tractography can be highly anatomically accurate—if we know where white matter pathways start, where they end, and where they do not go. Brain Struct Funct 225, 2387–2402. https://doi.org/10.1007/s00429-020-02129-z

Serra, L., D'Amelio, M., Di Domenico, C., Dipasquale, O., Marra, C., Mercuri, N.B., Caltagirone, C., Cercignani, M., Bozzali, M., 2018. In vivo mapping of brainstem nuclei functional connectivity disruption in Alzheimer's disease. Neurobiology of Aging 72, 72–82. https://doi.org/10.1016/j.neurobiolaging.2018.08.012

Simonini, M.V., Polak, P.E., Sharp, A., McGuire, S., Galea, E., Feinstein, D.L., 2010. Increasing CNS Noradrenaline Reduces EAE Severity. J Neuroimmune Pharmacol 5, 252–259. https://doi.org/10.1007/s11481-009-9182-2

Thompson, A.J., Banwell, B.L., Barkhof, F., Carroll, W.M., Coetzee, T., Comi, G., Correale, J., Fazekas, F., Filippi, M., Freedman, M.S., Fujihara, K., Galetta, S.L., Hartung, H.P., Kappos, L., Lublin, F.D., Marrie, R.A., Miller, A.E., Miller, D.H., Montalban, X., Mowry, E.M., Sorensen, P.S., Tintoré, M., Traboulsee, A.L., Trojano, M., Uitdehaag, B.M.J., Vukusic, S., Waubant, E., Weinshenker, B.G., Reingold, S.C., Cohen, J.A., 2018. Diagnosis of multiple sclerosis: 2017 revisions of the McDonald criteria. The Lancet Neurology 17, 162–173. https://doi.org/10.1016/S1474-4422(17)30470-2

Tortorella, P., Rocca, M.A., Colombo, B., Annovazzi, P., Comi, G., Filippi, M., 2006. Assessment of MRI abnormalities of the brainstem from patients with migraine and multiple sclerosis. Journal of the Neurological Sciences 244, 137–141. https://doi.org/10.1016/j.jns.2006.01.015

Tournier, J.-D., Calamante, F., Connelly, A., 2007. Robust determination of the fibre orientation distribution in diffusion MRI: Non-negativity constrained super-resolved spherical deconvolution. NeuroImage 35, 1459–1472. https://doi.org/10.1016/j.neuroimage.2007.02.016

Tournier, J.-D., Smith, R., Raffelt, D., Tabbara, R., Dhollander, T., Pietsch, M., Christiaens, D., Jeurissen, B., Yeh, C.-H., Connelly, A., 2019. MRtrix3: A fast, flexible and open software framework for medical image processing and visualisation. NeuroImage 202, 116137. https://doi.org/10.1016/j.neuroimage.2019.116137

Trapp, B.D., Stys, P.K., 2009. Virtual hypoxia and chronic necrosis of demyelinated axons in multiple sclerosis. The Lancet Neurology 8, 280–291. https://doi.org/10.1016/S1474-4422(09)70043-2

Watson, T.M., Ford, E., Worthington, E., Lincoln, N.B., 2014. Validation of Mood Measures for People with Multiple Sclerosis. International Journal of MS Care 16, 105–109. https://doi.org/10.7224/1537-2073.2013-013

Zielińska-Nowak, E., Włodarczyk, L., Kostka, J., Miller, E., 2020. New Strategies for Rehabilitation and Pharmacological Treatment of Fatigue Syndrome in Multiple Sclerosis.

**Figure Legend**

**Fig. 1** Main dopaminergic (left), noradrenergic (centre), and serotoninergic (right) pathways within the human central nervous system (top) and schematic of the monoaminergic connections that have been analysed in this study by tract of interest analysis (bottom). The colors of the different regions in the bottom are used in the later figures for the same regions. Figure was created with BioRender.com (SN = *substantia nigra*; VTA = ventral tegmental area; DS = dorsal striatum; $N_{acc}$ = nucleus accumbens; Hippoc = hippocampus; Amygd = amygdala; dl-PFC = dorsolateral prefrontal cortex; Of-PFC = orbitofrontal-PFC; LC = *locus coeruleus*; MR = median raphe; DR = dorsal raphe).

**Fig.2** Intermediate steps for sample tracts (left: cingulum; centre: locus coeruleus- dorsolateral prefrontal cortex; right: median raphe-cerebellar lobule VII). A) the tractogram reconstructed using the inclusion and exclusion criteria described in Supplementary Table 1; B) the related mask defined using an appropriate threshold; C) the related fixels representing the underlying fiber populations (P = posterior, R = right, LC = locus coeruleus, dlPFC = dorsolateral prefrontal cortex; MR = median raphe, Cer = cerebellar).

**Fig. 3** Mesocorticolimbic fibre tract-specific significant FDC decreases in patients with multiple sclerosis (RR-MS) compared to healthy control (HC). Tracts of interest projecting from ventral tegmental area (VTA) are shown in glass brain representations using the *mrview* tool in MRtrix3. A) mesolimbic pathway encompasses the tracts connecting VTA with nucleus accumbens, amygdala, and hippocampus; B) mesocortical pathway encompasses VTA projections to medial and lateral orbitofrontal and dorsolateral prefrontal cortex (PFC). Differences in average FDC between HC and RR-MS patients in the selected white matter tracts of the A) mesolimbic and B) mesocortical pathway are shown in scatter plots. Comparisons were tested by independent sample t-tests. The statistical threshold was set to $p<0.003$ after Bonferroni correction for multiple comparisons (FDC = fibre-density cross-section, A = anterior, L = left).

**Fig. 4** Locus coeruleus-prefrontal cortex fibre tract-specific significant FDC decreases in patients with multiple sclerosis (RR-MS) compared to healthy control (HC). Tracts of interest

projecting from locus coeruleus (LC) to medial and lateral orbitofrontal and dorsolateral prefrontal cortex (PFC) are shown in glass brain representations using the *mrview* tool in MRtrix3. Differences in average FDC between HC and RR-MS patients in the selected white matter tracts of the LC-PFC tracts are shown in scatter plots. Comparisons were tested by independent sample t-tests. The statistical threshold was set to $p<0.003$ after Bonferroni correction for multiple comparisons (FDC = fibre-density cross-section, A = anterior, L = left, R = right).

**Fig. 5** Raphe nuclei-cerebellar cortex fibre tract-specific significant FDC decreases in patients with multiple sclerosis (RR-MS) compared to healthy control (HC). Tracts of interest projecting from A) median raphe (MR) and B) dorsal raphe (DR) to cerebellum are shown in glass brain representations using the *mrview* tool in MRtrix3. Differences in average FDC between HC and MS patients in the selected white matter tracts from raphe nuclei to cerebellar lobules V-VI and VII are shown in scatter plots. Comparisons were tested by independent sample t-tests. The statistical threshold was set to $p<0.003$ after Bonferroni correction for multiple comparisons. (FDC = fibre-density cross-section, A = anterior, P = posterior, L = left, R = right).

**Fig. 6** White matter lesions probability map in MS patients. Each participant's lesion maps were averaged to yield a lesion probability map where each voxel value represents the probability of it being a lesion (expressed as percentage). Results are superposed on the MNI-T1 template using the *FSLeyes* tool in FSL (R = right).

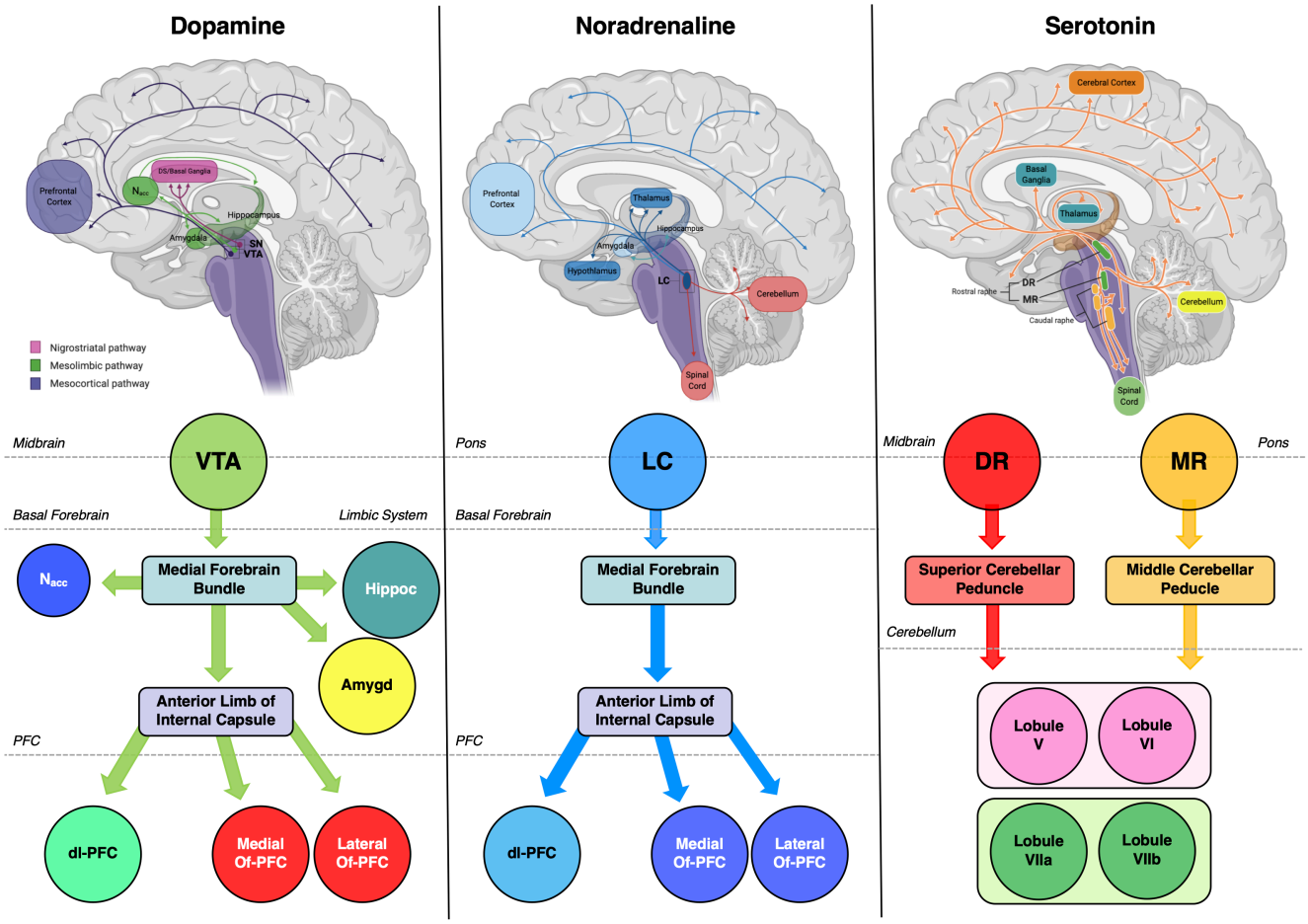
Dopamine
Noradrenaline
Serotonin
Prefrontal Cortex
DS/Basal Ganglia
Nacc
Hippocampus
Amygdala
SN
VTA
Nigrostriatal pathway
Mesolimbic pathway
Mesocortical pathway
Thalamus
Hypothlamus
LC
Cerebellum
Spinal Cord
Cerebral Cortex
Basal Ganglia
Rostral raphe
DR
MR
Caudal raphe
Midbrain
VTA
Basal Forebrain
Limbic System
Nacc
Medial Forebrain Bundle
Hippoc
Amygd
Anterior Limb of Internal Capsule
PFC
dl-PFC
Medial Of-PFC
Lateral Of-PFC
Pons
LC
Medial Forebrain Bundle
Anterior Limb of Internal Capsule
PFC
dl-PFC
Medial Of-PFC
Lateral Of-PFC
Midbrain
DR
Pons
MR
Superior Cerebellar Peduncle
Middle Cerebellar Peducle
Cerebellum
Lobule V
Lobule VI
Lobule VIIa
Lobule VIIb

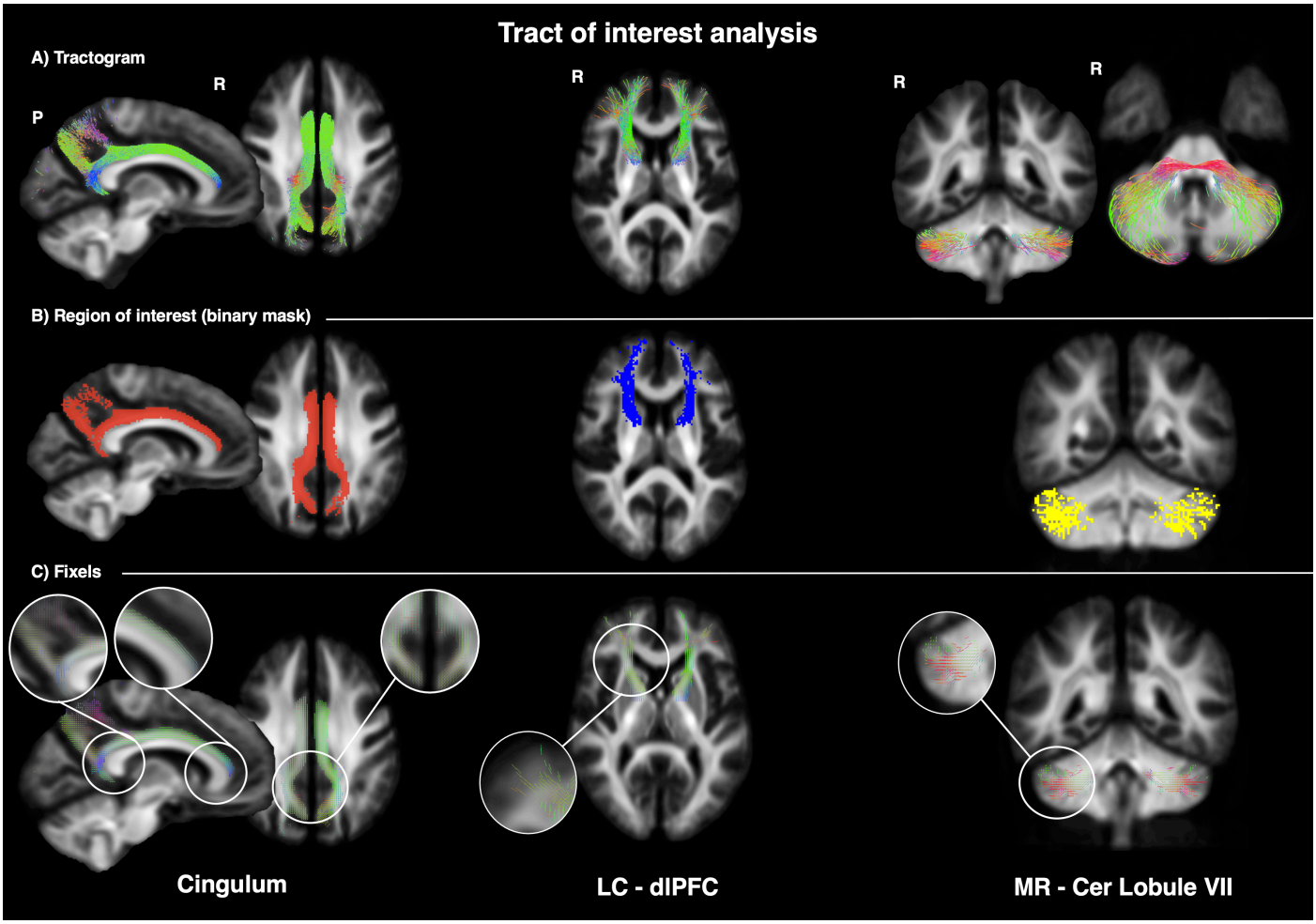
Tract of interest analysis
A) Tractogram
R
P
R
R
R
B) Region of interest (binary mask)
C) Fixels
Cingulum
LC - dlPFC
MR - Cer Lobule VII

# Ventral Tegmental Area

## A) MESOLIMBIC PATHWAY

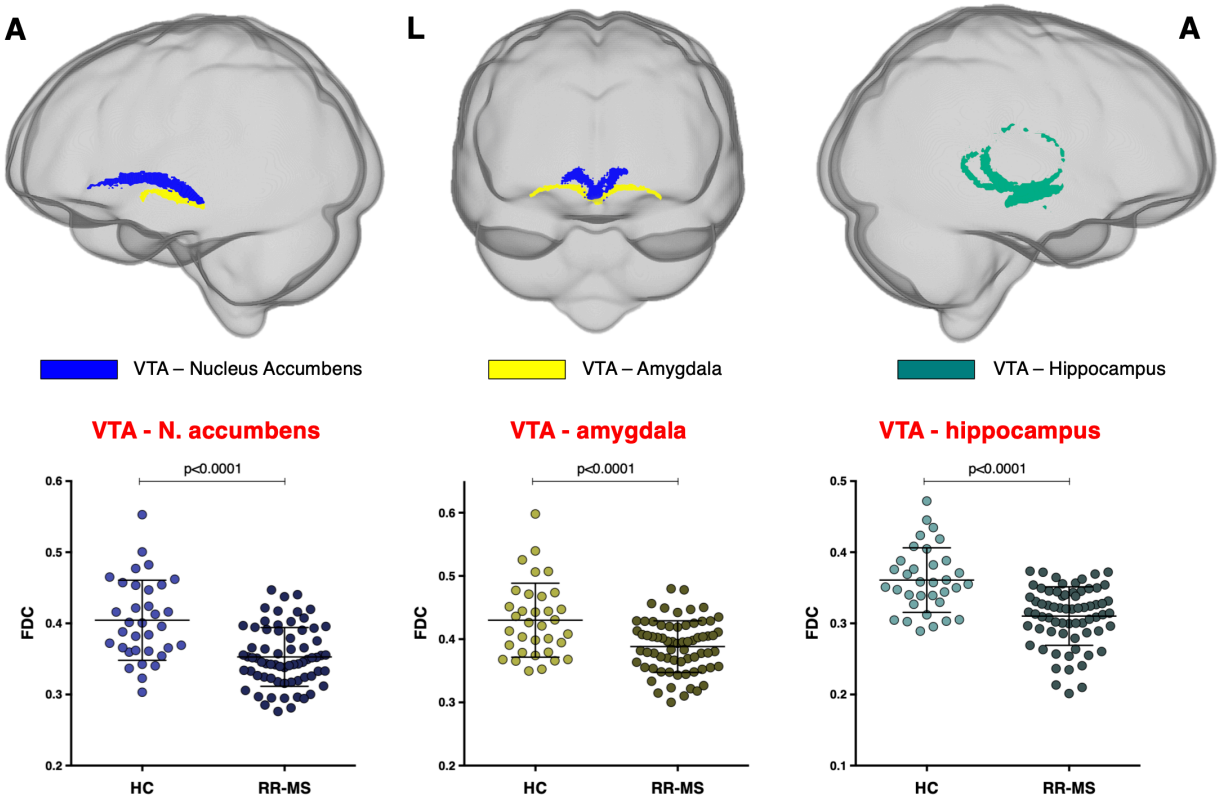


## B) MESOCORTICAL PATHWAY

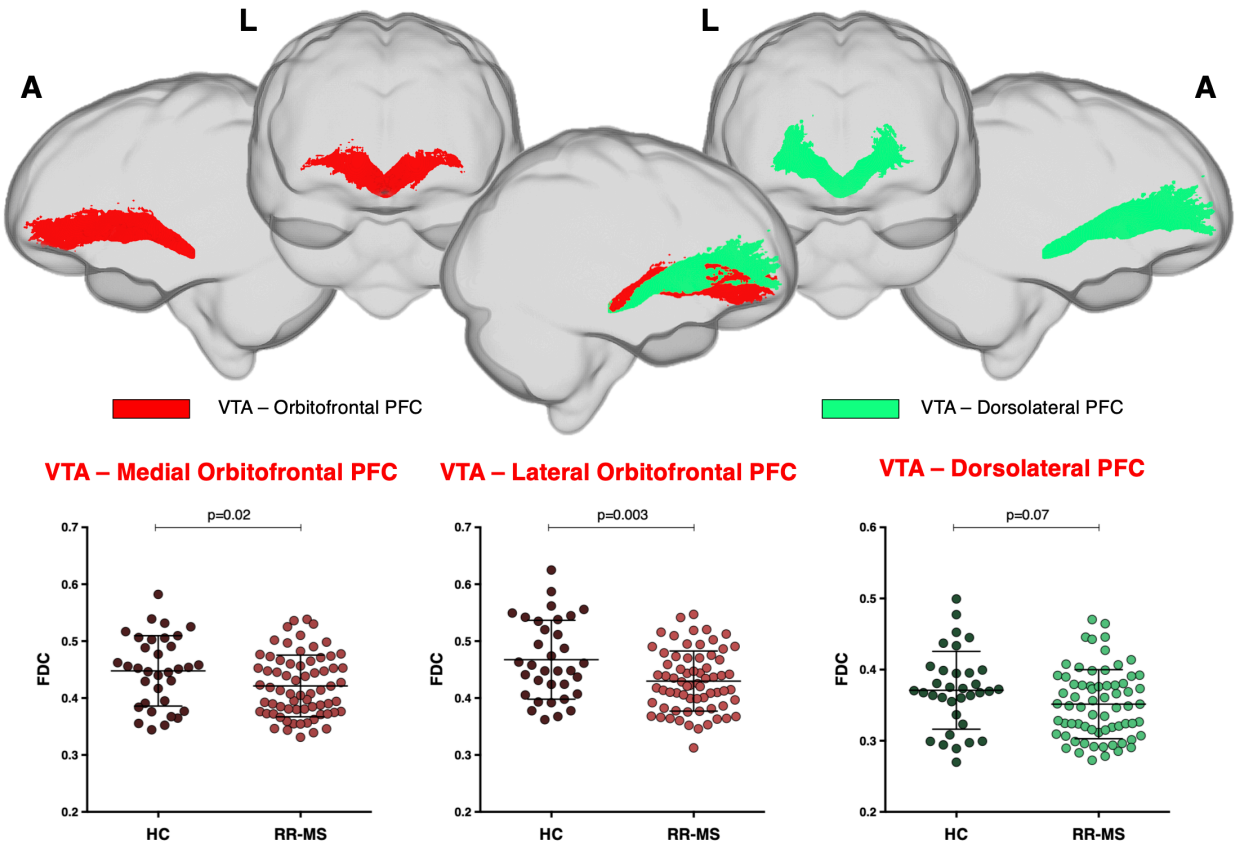

# Locus Coeruleus

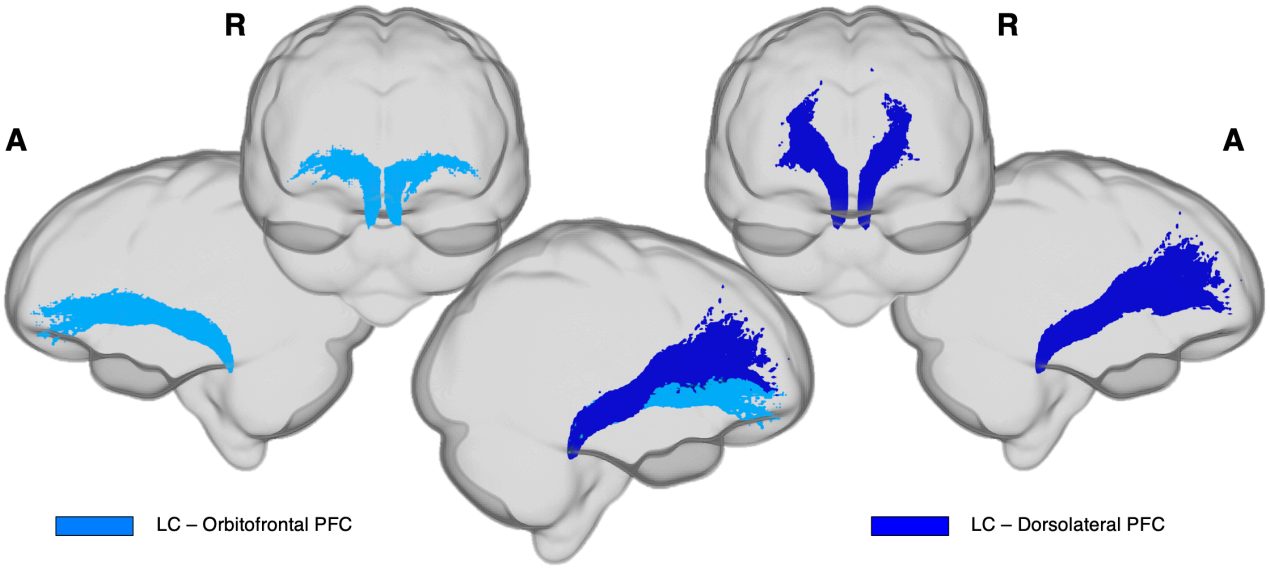


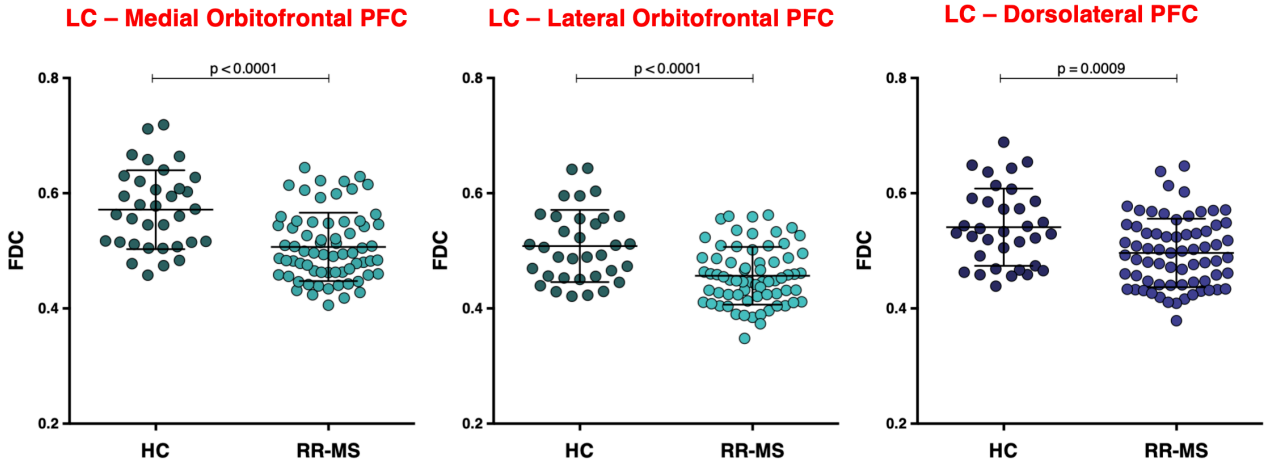

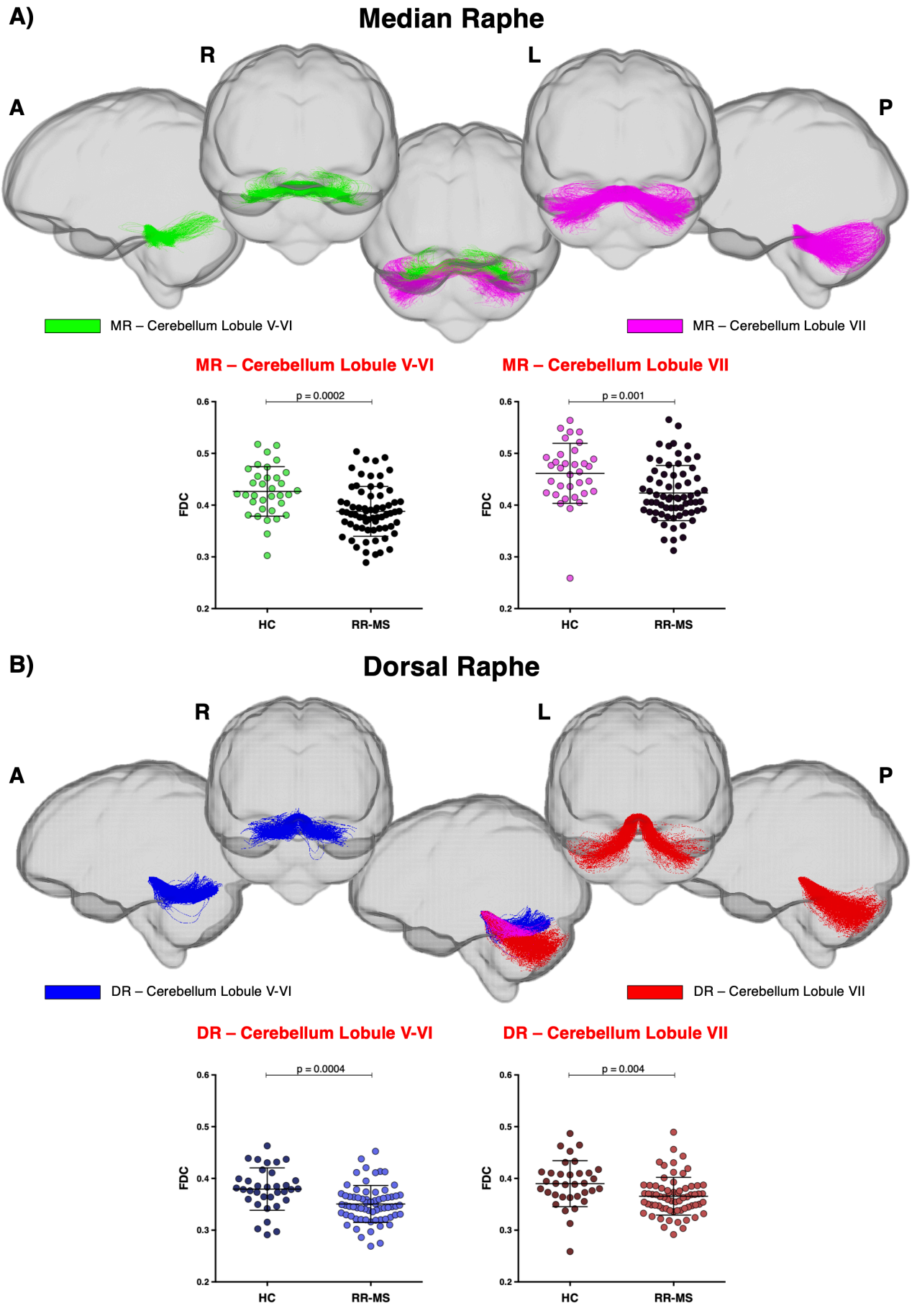
A)
Median Raphe
R
L
A
P
MR – Cerebellum Lobule V-VI
MR – Cerebellum Lobule VII
MR – Cerebellum Lobule V-VI
MR – Cerebellum Lobule VII
p = 0.0002
p = 0.001
FDC
0.6
0.5
0.4
0.3
0.2
HC
RR-MS
B)
Dorsal Raphe
R
L
A
P
DR – Cerebellum Lobule V-VI
DR – Cerebellum Lobule VII
DR – Cerebellum Lobule V-VI
DR – Cerebellum Lobule VII
p = 0.0004
p = 0.004
FDC
0.6
0.5
0.4
0.3
0.2
HC
RR-MS

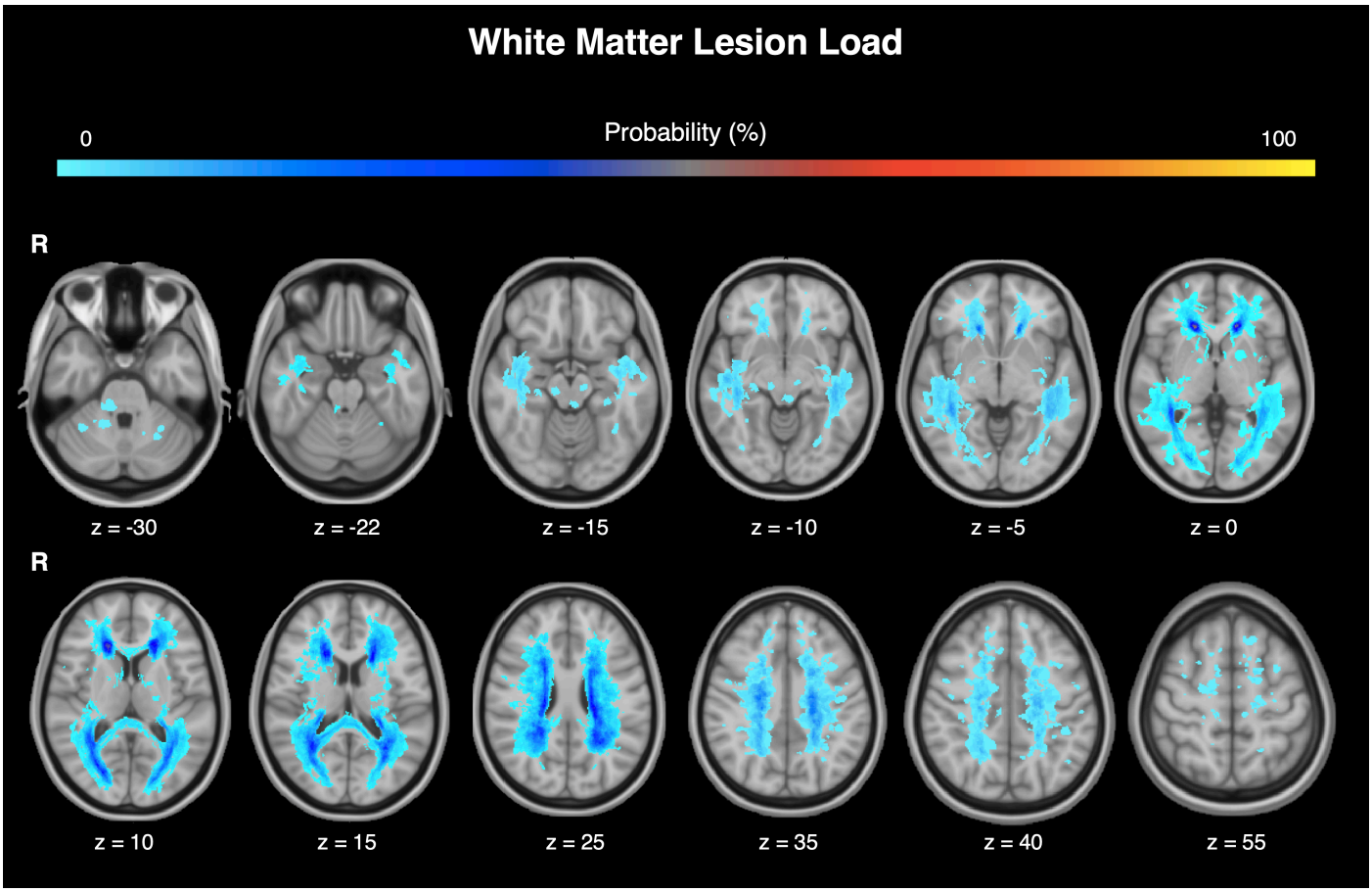
White Matter Lesion Load
0
Probability (%)
100
R
z = -30
z = -22
z = -15
z = -10
z = -5
z = 0
R
z = 10
z = 15
z = 25
z = 35
z = 40
z = 55

**Table 1**

Main demographic and clinical characteristics of the included population.

| | **RR-MS** | **HC** | ***p*** |
|---|---|---|---|
| n | 68 | 34 | |
| Age, years, mean±SD | 43.3±7.7 | 43.9±15.9 | *0.78* |
| Female, number (percentage) | 43 (63.2) | 19 (55.9) | *0.47* |
| Disease duration, years, mean±SD | 7.4±6.5 | | |
| EDSS, median (1st-3rd quartiles) | 1.5 (1.0-3.0) | | |
| MS-specific treatment, number (percentage) | | | |
| *No treatment* | 16 (23.5) | | |
| *First line DMTs* | 25 (36.8) | | |
| *Second line DMTs* | 27 (39.7) | | |
| MFIS-Tot, median (1st-3rd quartiles) | 34.5 (24.5-47.0) | | |
| *MFIS-Cog* | 16.0 (11.0-20.0) | | |
| *MFIS-Phys* | 16.7 (10.0-23.0) | | |
| *MFIS-PS* | 3.0 (1.0-4.0) | | |
| SDMT, median (1st-3rd quartiles) | 49.0 (48.2-64.7) | | |
| HADS-D, median (1st-3rd quartiles) | 1.5 (1.0-4.0) | | |
| ESS, median (1st-3rd quartiles) | 4.0 (2.0-6.2) | | |

[Abbreviations = RR-MS: Relapsing-Remitting Multiple Sclerosis; HC: Healthy Controls; SD: standard deviation; EDSS: Expanded Disability Status Scale; DMTs: Disease Modifying Therapies; MFIS: Modified Fatigue Impact Scale; Tot: total score; Cog: cognitive subscale; Phys: physical subscale; PS: psychosocial subscale; SDMT: Symbol Digit Modalities Test; HADS-D: Hospital Anxiety Depression Scale; ESS: Epworth Sleepiness Scale.]

## Table 2

Average values of fibre density (FD), fibre cross-section (FC), and fibre density and cross-section (FDC) in the selected fibre tracts in relapsing-remitting multiple sclerosis (RR-MS) patients and in healthy controls (HC). Data are reported as mean ± standard deviation. Statistical threshold was set to $p<0.003$ after Bonferroni correction for multiple comparisons. *FC data are expressed as logarithm of FC values ($_{log}$FC) to ensure that data were centred around zero and normally distributed.

| **Tract** | **FD** | | | **$_{log}$FC*** | | | **FDC** | | |
|---|---|---|---|---|---|---|---|---|---|
| | **RR-MS** | **HC** | *p* | **RR-MS** | **HC** | *p* | **RR-MS** | **HC** | *p* |
| **VTA-$N_{acc}$** | 0.34±0.02 | 0.36±0.03 | **<0.0001** | 0.02±0.08 | 0.09±0.07 | **0.0001** | 0.35±0.04 | 0.40±0.06 | **<0.0001** |
| **VTA-amygdala** | 0.38±0.02 | 0.40±0.03 | 0.006 | -0.01±0.06 | 0.05±0.06 | **<0.0001** | 0.39±0.04 | 0.43±0.06 | **<0.0001** |
| **VTA-hippocampus** | 0.32±0.04 | 0.35±0.03 | **0.0004** | -0.01±0.09 | 0.03±0.07 | 0.07 | 0.31±0.04 | 0.36±0.04 | **<0.0001** |
| **VTA-dlPFC** | 0.33±0.02 | 0.33±0.01 | 0.83 | 0.04±0.10 | 0.09±0.10 | 0.06 | 0.35±0.04 | 0.37±0.05 | 0.07 |
| **VTA-mOfPFC** | 0.39±0.02 | 0.39±0.03 | 0.74 | 0.05±0.09 | 0.10±0.08 | 0.003 | 0.42±0.05 | 0.45±0.06 | 0.02 |
| **VTA-lOfPFC** | 0.41±0.02 | 0.42±0.03 | 0.07 | 0.04±0.10 | 0.10±0.09 | 0.003 | 0.43±0.05 | 0.47±0.07 | 0.003 |
| **LC-dlPFC** | 0.48±0.02 | 0.49±0.03 | 0.05 | 0.02±0.09 | 0.08±0.08 | **0.001** | 0.49±0.06 | 0.54±0.07 | **0.0009** |
| **LC-mOfPFC** | 0.49±0.02 | 0.51±0.03 | **0.0009** | 0.02±0.08 | 0.10±0.08 | **<0.0001** | 0.50±0.06 | 0.57±0.07 | **<0.0001** |
| **LC-lOfPFC** | 0.45±0.02 | 0.46±0.03 | 0.007 | 0.03±0.08 | 0.09±0.08 | **0.0001** | 0.46±0.05 | 0.51±0.06 | **<0.0001** |
| **MR-Cer Lob VII** | 0.38±0.01 | 0.38±0.02 | 0.42 | 0.10±0.09 | 0.16±0.10 | 0.007 | 0.42±0.05 | 0.46±0.06 | **0.001** |
| **MR-Cer Lob V+VI** | 0.35±0.01 | 0.36±0.01 | 0.06 | 0.06±0.08 | 0.12±0.08 | **0.001** | 0.39±0.05 | 0.43±0.05 | **0.0002** |
| **DR-Cer Lob VII** | 0.35±0.02 | 0.35±0.02 | 0.80 | 0.05±0.08 | 0.10±0.09 | 0.005 | 0.36±0.04 | 0.39±0.04 | 0.004 |
| **DR-Cer Lob V+VI** | 0.35±0.02 | 0.35±0.02 | 0.49 | 0.02±0.07 | 0.08±0.08 | **0.001** | 0.35±0.03 | 0.38±0.04 | **0.0004** |
| **Cingulum** | 0.34±0.02 | 0.34±0.02 | 0.07 | 0.01±0.10 | 0.07±0.09 | 0.005 | 0.35±0.05 | 0.37±0.05 | 0.08 |

[Abbreviations: VTA: ventral tegmental area; $N_{acc}$: nucleus accumbens; dlPFC: dorsolateral prefrontal cortex; mOfPFC: medial orbito-frontal prefrontal cortex; lOfPFC: lateral orbito-frontal prefrontal cortex; LC: locus coeruleus; Cer Lob: Cerebellar Lobule; MR: median raphe; DR: dorsal raphe]

## Supplementary Files

**Supplementary Table 1: Tractograms generated using MRtrix.** All probabilistic tractographies were performed unidirectionally, with minimum length of 10 mm and maximum length of 250 mm. We used exclusion criteria by means of tailored region of interest (ROI) that were created using the Harvard-Oxford cortical and structural atlases for cerebral cortex and subcortical structures [17], and the probabilistic atlas of the human cerebellum for cerebellar cortex [18], both distributed with FMRIB Software Library (FSL). The following 14 tracts were reconstructed: ventral tegmental area (VTA)-Nucleus accumbens; VTA-amygdala; VTA-hippocampus; VTA-dorsolateral(dl) prefrontal cortex (PFC); VTA-medial orbitofrontal(mOf)PFC; VTA-lateral orbitofrontal(lOf)PFC; locus coeruleus (LC)-dlPFC; LC-mOfPFC; LC-lOfPFC; median raphe (M)R-Cerebellar Lobule V-VI; MR-Cerebellar Lobule VII; dorsal raphe (DR)-Cerebellar lobule V-VI; DR-Cerebellar lobule VII; cingulum. Averaged FD, FC, and FDC were calculated across the fixels in each tract in MS patients and HC.

| **Tract** | **Angular threshold** | **Number of streamlines** | **Exclusion criteria** |
|---|---|---|---|
| VTA-$N_{acc}$ | 20° | 100 | PFC, PCC, corpus callosum |
| VTA-amygdala | 20° | 100 | Temporal lobe, hippocampus |
| VTA-hippocampus | 20° | 100 | Temporal lobe, amygdala |
| VTA-dlPFC | 20° | 1000 | lOfPFC, mOfPFC, ACC, corpus callosum, temporal and parietal lobes, thalamus |
| VTA-mOfPFC | 20° | 500 | lOfPFC, dlPFC, ACC, temporal and parietal lobes, thalamus, $N_{acc}$ |
| VTA-lOfPFC | 20° | 500 | mOfPFC, dlPFC, temporal lobe, parietal lobe, thalamus, $N_{acc}$ |
| LC-dlPFC | 20° | 1000 | lOfPFC, mOfPFC, ACC, corpus callosum, temporal and parietal lobes, thalamus |
| LC-mOfPFC | 20° | 500 | lOfPFC, dlPFC, ACC, temporal and parietal lobes, thalamus, $N_{acc}$ |
| LC-lOfPFC | 20° | 500 | mOfPFC, dlPFC, temporal and parietal lobes, thalamus, $N_{acc}$ |
| MR-Cer Lob VII | 10° | 1000 | / |

| | | | |
|---|---|---|---|
| MR-Cer Lob V+VI | 10° | 1000 | Cer Lob VII |
| DR-Cer Lob VII | 10° | 1000 | / |
| DR-Cer Lob V+VI | 10° | 1000 | Cer Lob VII |
| Cingulum | 20° | 10.000 | Temporal lobe, hippocampus, corpus callosum |

Abbreviations = VTA: ventral tegmental area; $N_{acc}$: nucleus accumbens; dlPFC: dorso-lateral prefrontal cortex; mOfPFC: medial orbito-frontal prefrontal cortex; lOfPFC: lateral orbito-frontal prefrontal cortex; PCC: posterior cingulate, cortex; ACC: anterior cingulate cortex; LC: locus coeruleus; MR: median raphe; DR: dorsal raphe; Cer Lob: Cerebellar Lobule.

**Supplementary Table 2: Correlations between fibre density and cross-section (FDC) and fatigue scores.** Correlations between FDC in the selected fibre tracts in relapsing-remitting multiple sclerosis patients and fatigue scores, as computed by the total score of the Modified Fatigue Impact Scale (MFIS-Tot), which is obtained by adding the scores of the MFIS subscales: cognitive (MFIS-Cog), physical (MFIS-Phys) and psychosocial (*not shown*). Correlations between FDC and MFIS scores were performed assessing the Pearson correlation coefficient (r). Statistical threshold was set to $p<0.025$ after Bonferroni correction for multiple comparisons.

| Tract | MFIS-Tot | | MFIS-Cog | | MFIS-Phys | |
|---|---|---|---|---|---|---|
| | r | *p* | r | *p* | r | *p* |
| **FDC VTA-$N_{acc}$** | -0,19 | 0,126 | **-0,28** | **0,021** | 0,14 | 0,248 |
| **FDC VTA-amygdala** | -0,21 | 0,090 | **-0,27** | **0,017** | -0,03 | 0,796 |
| **FDC VTA-hippocampus** | **-0,32** | **0,008** | **-0,36** | **0,002** | -0,05 | 0,662 |
| **FDC VTA-dlPFC** | -0,15 | 0,237 | -0,25 | 0,037 | 0,09 | 0,475 |
| **FDC VTA-mOfPFC** | -0,14 | 0,272 | -0,25 | 0,040 | 0,06 | 0,610 |
| **FDC VTA-lOfPFC** | -0,16 | 0,185 | **-0,30** | **0,014** | 0,05 | 0,688 |
| **FDC LC-dlPFC** | -0,16 | 0,180 | **-0,29** | **0,017** | 0,07 | 0,585 |
| **FDC LC-mOfPFC** | -0,15 | 0,219 | -0,26 | 0,031 | 0,04 | 0,773 |
| **FDC LC-lOfPFC** | -0,15 | 0,219 | **-0,28** | **0,019** | 0,06 | 0,601 |
| **FDC MR-Cer Lob VII** | -0,17 | 0,164 | -0,27 | 0,025 | 0,21 | 0,084 |
| **FDC MR-Cer Lob V+VI** | -0,13 | 0,275 | -0,22 | 0,068 | 0,17 | 0,173 |
| **FDC DR-Cer Lob VII** | -0,10 | 0,419 | -0,14 | 0,244 | 0,18 | 0,146 |
| **FDC DR-Cer Lob V+VI** | -0,03 | 0,818 | -0,07 | 0,569 | 0,24 | 0,052 |
| **Cingulum** | -0,22 | 0,066 | **-0,34** | **0,004** | 0,09 | 0,471 |

[Abbreviations: MFIS: Modified Fatigue Impact Scale; Tot: total score; Cog: cognitive subscale; Phys: physical subscale; FDC: fibre density and cross-section; VTA: ventral tegmental area; $N_{acc}$: nucleus accumbens; dlPFC: dorsolateral prefrontal cortex; mOfPFC: medial orbito-frontal prefrontal cortex; lOfPFC: lateral orbito-frontal prefrontal cortex; LC: locus coeruleus; Cer Lob: Cerebellar Lobule; MR: median raphe; DR: dorsal raphe]

**Supplementary Table 3: Partial correlations between fibre density and cross-section (FDC) and fatigue scores, controlling for depression and sleep disturbances.** Partial correlations (controlled for the scores of Hospital Anxiety and Depression Scale [HADS-D] and the Epworth Sleepiness Scale [ESS]) between FDC in the selected fibre tracts in relapsing-remitting multiple sclerosis patients and fatigue scores, as computed by the total score of the Modified Fatigue Impact Scale (MFIS-Tot), which is obtained by adding the scores of the MFIS subscales: cognitive (MFIS-Cog), physical (MFIS-Phys) and psychosocial (*not shown*). Partial correlations between FDC and MFIS scores were performed assessing the Pearson correlation coefficient (r), controlling for HADS-D and ESS. Statistical threshold was set to $p<0.025$ after Bonferroni correction for multiple comparisons.

| **Tract** | **MFIS-Tot** | | **MFIS-Cog** | | **MFIS-Phys** | |
|---|---|---|---|---|---|---|
| | **r** | ***p*** | **r** | ***p*** | **r** | ***p*** |
| **FDC VTA-$N_{acc}$** | -0,19 | 0,121 | **-0,27** | **0,025** | 0,08 | 0,530 |
| **FDC VTA-amygdala** | -0,21 | 0,088 | **-0,28** | **0,021** | -0,09 | 0,447 |
| **FDC VTA-hippocampus** | **-0,32** | **0,008** | **-0,36** | **0,002** | -0,07 | 0,587 |
| **FDC VTA-dlPFC** | -0,15 | 0,240 | -0,24 | 0,055 | 0,00 | 0,990 |
| **FDC VTA-mOfPFC** | -0,14 | 0,271 | -0,24 | 0,054 | -0,01 | 0,923 |
| **FDC VTA-lOfPFC** | -0,17 | 0,179 | **-0,29** | **0,020** | -0,03 | 0,776 |
| **FDC LC-dlPFC** | -0,17 | 0,170 | **-0,28** | **0,022** | -0,02 | 0,867 |
| **FDC LC-mOfPFC** | -0,16 | 0,198 | -0,26 | 0,033 | -0,02 | 0,855 |
| **FDC LC-lOfPFC** | -0,16 | 0,204 | **-0,28** | **0,023** | -0,02 | 0,877 |
| **FDC MR-Cer Lob VII** | -0,17 | 0,168 | -0,26 | 0,040 | 0,13 | 0,297 |
| **FDC MR-Cer Lob V+VI** | -0,13 | 0,276 | -0,21 | 0,091 | 0,10 | 0,400 |
| **FDC DR-Cer Lob VII** | -0,09 | 0,444 | -0,11 | 0,356 | 0,09 | 0,466 |
| **FDC DR-Cer Lob V+VI** | -0,02 | 0,851 | -0,06 | 0,711 | 0,18 | 0,145 |
| **Cingulum** | -0,23 | 0,067 | **-0,33** | **0,006** | 0,03 | 0,791 |

[Abbreviations: MFIS: Modified Fatigue Impact Scale; Tot: total score; Cog: cognitive subscale; Phys: physical subscale; FDC: fibre density and cross-section; VTA: ventral tegmental area; $N_{acc}$: nucleus accumbens; dlPFC: dorsolateral prefrontal cortex; mOfPFC: medial orbito-frontal prefrontal cortex; lOfPFC: lateral orbito-frontal prefrontal cortex; LC: locus coeruleus; Cer Lob: Cerebellar Lobule; MR: median raphe; DR: dorsal raphe]

**Supplementary Fig.1: Cingulum fibre tract-specific significant FDC decreases in patients with multiple sclerosis (RR-MS) compared to healthy control (HC).** The cingulum – connecting the anterior cingulate cortex with posterior cingulate cortex – is shown in glass brain representations using the *mrview* tool in MRtrix3. Differences in average FDC between HC and RR-MS patients in the cingulum is shown in scatter plots. Comparisons were tested by independent sample t-tests. The statistical threshold was set to $p<0.003$ after Bonferroni correction for multiple comparisons (FDC = fibre-density cross-section, A = anterior, L = left, R = right).

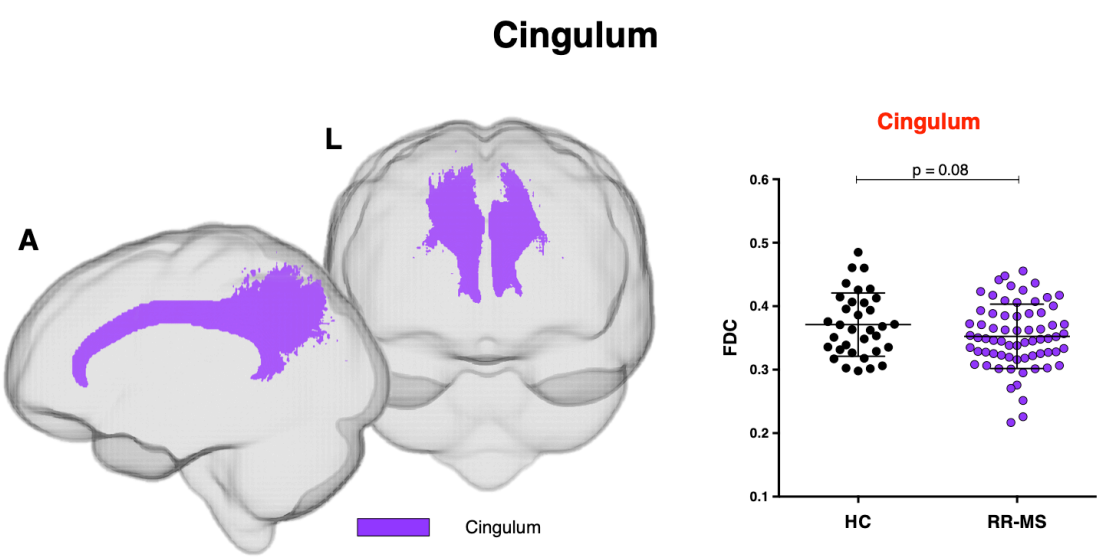

**Supplementary Figure 2: Differences in regional grey matter atrophy between MS patients and healthy controls.** Voxel-based morphometry analysis displayed significant grey matter loss in bilateral thalamus in MS patients, as compared to healthy controls. Results are reported at $p_{FWE}<0.05$, corrected at peak level and are overlaid on the MNI_T1 template using the *FSLeyes* tool in FSL (P = posterior, R = right).